The Company of Biologists

RESEARCH ARTICLE

Side branching and luminal lineage commitment by ID2 in developing mammary glands

Jinwoo Seong[1], Nam-Shik Kim[1], Jee-Ah Kim[1], Wonbin Lee[1], Ji-Yun Seo[1], Min Kyu Yum[1], Ji-Hoon Kim[1], Inkuk Park[1], Jong-Seol Kang[1], Sung-Hwan Bae[1], Cheol-Heui Yun[2] and Young-Yun Kong[1],*

ABSTRACT

Mammary glands develop through primary ductal elongation and side branching to maximize the spatial area. Although primary ducts are generated by bifurcation of terminal end buds, the mechanism through which side branching occurs is still largely unclear. Here, we show that inhibitor of DNA-binding 2 (ID2) drives side branch formation through the differentiation of K6$^+$ bipotent progenitor cells (BPs) into CD61$^+$ luminal progenitor cells (LPs). *Id2*-null mice had side-branching defects, along with developmental blockage of the differentiation of K6$^+$ BPs into CD61$^+$ LPs. Notably, CD61$^+$ LPs were found in budding and side branches, but not in terminal end buds. Hormone reconstitution studies using ovariectomized MMTV-hemagglutinin-nuclear localized sequence-tagged *Id2* transgenic mice revealed that ID2 is a key mediator of progesterone, which drives luminal lineage differentiation and side branching. Our results suggest that CD61 is a marker of side branches and that ID2 regulates side branch formation by inducing luminal lineage commitment from K6$^+$ BPs to CD61$^+$ LPs.

INTRODUCTION

During adolescence, mammary glands gradually differentiate into mature glands through the functions of ovarian hormones, such as estrogen and progesterone (Howlin et al., 2006; Robinson, 2007). Primary ducts of mammary glands have a proliferative mass of cells, called terminal end buds (TEBs), which progressively fill fat pads through bifurcation. Along with primary ductal elongation, new branches bud out laterally from the primary ducts; this process is called lateral or side branching. Given that side branching has to occur to enable adequate production of milk during lactation, many studies have evaluated how ovarian hormones affect side branching. Progesterone receptor (PGR)-null (*Pgr*$^{-/-}$) mice exhibit fewer side branches compared with controls, and transplanted mammary epithelial cells (MECs) from *Pgr*$^{-/-}$ ducts into cleared fat pads show defects in side branching (Brisken et al., 2000; Lydon et al., 1995; Soyal et al., 2002). By contrast, progesterone pellet treatment in peripubertal mice enhances side branching (Atwood et al., 2000), indicating that progesterone is a key regulator of side branching.

To date, many studies have revealed factors that control the formation of side branches, including progesterone and its downstream mediator, receptor activator of nuclear factor-κB ligand (RANKL) (Beleut et al., 2010; Brisken et al., 2000; Fernandez-Valdivia et al., 2009; Mukherjee et al., 2010; Rajaram et al., 2015). However, the mechanisms through which side branches are formed still require further investigation.

Mammary stem cells (MaSCs) differentiate into bipotent progenitor cells (BPs) that further differentiate into either luminal or myoepithelial progenitor cells (Brisken and Duss, 2007; Hennighausen and Robinson, 2005; Visvader and Stingl, 2014). CD61 (integrin-β3) has been suggested as a marker of luminal progenitor cells (LPs) (Asselin-Labat et al., 2007), which differentiate into mature luminal cells, namely ductal and alveolar cells. E74-like factor 5 (ELF5) and GATA-3 induce terminal luminal differentiation of CD61$^+$ LPs into alveolar cells (Chakrabarti et al., 2012; Choi et al., 2009; Cui et al., 2004; Kouros-Mehr et al., 2006; Lee et al., 2013; Oakes et al., 2008), and pregnant *Cd61*-null mice show defects in lobuloalveologenesis (Desgrosellier et al., 2014), suggesting that CD61 is essential for luminal lineage differentiation. Although many researchers have demonstrated the importance of CD61$^+$ LPs in luminal lineage differentiation, the factors inducing the differentiation of stem cells and/or BPs into CD61$^+$ LPs remain to be determined.

There are four different forms of Inhibitor of DNA-binding (ID) protein: ID1, ID2, ID3 and ID4. Although they all have a helix-loop-helix (HLH) domain (Norton et al., 1998), their respective functions in mammary glands differ. *Id1* or *Id3* single null mice show normal mammary gland development (de Candia et al., 2004; Lyden et al., 1999), whereas ID4 is a key regulator of MaSC self-renewal in basal cells (Best et al., 2014; Dong et al., 2011; Junankar et al., 2015). ID2 is highly expressed during pregnancy, and *Id2*$^{-/-}$ mice have defects in lobuloalveologenesis and induction of milk protein genes at pregnancy (de Candia et al., 2004; Miyoshi et al., 2002; Mori et al., 2003; Mori et al., 2000; Parrinello et al., 2001; Yokota et al., 1999; Yokota et al., 2001). Based on phenocopy between *Id2*$^{-/-}$ and *Rankl*$^{-/-}$ mice at pregnancy, we previously reported that RANKL drives nuclear retention of ID2 in MECs, and forced nuclear retention of ID2 rescues luminal differentiation defects in *Rankl*$^{-/-}$ mice (Kim et al., 2006, 2011). Given that RANKL is a key mediator of progesterone in side branching and the expansion of luminal cells (Beleut et al., 2010; Fata et al., 2000; Fernandez-Valdivia et al., 2009; Mukherjee et al., 2010; Obr et al., 2013), ID2 might be a putative downstream mediator of the progesterone/RANK signaling axis for side branching and luminal lineage commitment.

In this study, we found that ID2 stimulates side branch formation by inducing the differentiation of K6$^+$ BPs into CD61$^+$ LPs in virgin mammary glands. *Id2*$^{-/-}$ mice showed accumulation of K6$^+$ BPs and dramatic reduction of CD61$^+$ LPs with few side branches, whereas MMTV-hemagglutinin (*HA*)-nuclear localized sequence (*NLS*)-tagged *Id2* transgenic (*NLS-Id2* Tg) mice showed prolific induction

[1]School of Biological Sciences, College of Natural Sciences, Seoul 151-742, Republic of Korea. [2]Department of Agricultural Biotechnology, College of Agriculture and Life Sciences, Seoul National University, Seoul 151-742, Republic of Korea.

*Author for correspondence (ykong@snu.ac.kr)

Y.-Y.K., 0000-0001-7335-3729

DEVELOPMENT

1

of side branching. Importantly, most CD61$^+$ LPs were found in budding and side branches, but were rarely detected in primary ducts and TEBs, indicating that differentiation of CD61$^+$ LPs is involved in side branch formation rather than in primary ductal elongation. Hormone reconstitution studies using an ovariectomized (Ovx) *NLS-Id2* Tg mouse model revealed that nuclear ID2 is a downstream mediator of progesterone for side branching and luminal lineage differentiation. Our study provides crucial insights into how side branches are formed in developing virgin mammary glands.

RESULTS

Side-branching defects in *Id2$^{-/-}$* virgin mice

Previous studies reported that nulliparous *Id2$^{-/-}$* female mice had normal ductal trees, but showed defects in lobuloalveologenesis during pregnancy (Miyoshi et al., 2002; Mori et al., 2000). Given that lobuloalveolar cells are differentiated from LPs (Brisken and Duss, 2007; Hennighausen and Robinson, 2005; Visvader and Stingl, 2014), we hypothesized that the lobuloalveologenesis defects of *Id2$^{-/-}$* mice during pregnancy might be secondary defects caused by impaired luminal lineage differentiation in virgins. Hence, we carefully re-examined the development and morphogenesis of virgin *Id2$^{-/-}$* mammary glands. Consistent with previous reports, whole-mount Carmine-Alum (C-A) staining of mammary glands from 4- and 8-week-old virgin *Id2$^{-/-}$* mice showed intact TEBs and normal fat pad coverage of primary and secondary ducts (ducts formed by bifurcation of TEBs), similar to wild-type mice (Fig. 1E and data not shown). Interestingly, the number of tertiary branches (terminal side branches) were dramatically reduced in virgin *Id2$^{-/-}$* mice (0.11-fold) (Fig. 1A-I and Fig. S1A-E). We also quantified nascent side branches (the points at which side branches will bud out), which are identified through deeply colored spots in C-A staining (Sternlicht et al., 2006). Hematoxylin and Eosin (H&E) and C-A staining of mammary glands showed that *Id2$^{-/-}$* mammary glands exhibited few deeply colored nascent side branches (hereafter, nascent branches) and budding side branches (hereafter, budding branches), but showed an intact terminal end bud structure (Fig. 1A-K). The side-branching defects were evident, even at 20 weeks of age (Fig. S1F-K), indicating that side-branching defects in *Id2$^{-/-}$* mice do not result from the delayed development of mammary glands.

To investigate whether the side-branching defects in *Id2$^{-/-}$* mice were cell intrinsic or extrinsic (e.g. hormones or niches), we performed transplantation experiments. MECs from 8-week-old wild-type and *Id2$^{-/-}$* mice were transplanted into the cleared fat pads of 3-week-old wild-type mice (Fig. S1L). Eight weeks after transplantation, MECs from both genotypes repopulated well in the cleared fat pads. However, tertiary and nascent and/or budding branches were dramatically decreased in *Id2$^{-/-}$* donor transplants compared with those of controls (Fig. 1L-P). Taken together, our results showed that ID2 is required for the side branching of mammary glands in a cell-intrinsic manner.

Impaired differentiation into LPs in *Id2$^{-/-}$* mice

To identify the detailed phenotypes of *Id2$^{-/-}$* virgin mice, we examined ID2 expression patterns and the cellular composition of *Id2$^{-/-}$* mammary glands. ID2 was dominantly detected in luminal cells (96.80±2.19%) but barely in basal and/or myoepithelial cells (2.03±1.19%) (Fig. 2A,A′). Quantitative RT-PCR (qRT-PCR) analysis using freshly isolated MECs showed that the expression levels of luminal markers [i.e. cytokeratin 8 (*K8*), cytokeratin 18 (*K18*) and cytokeratin 19 (*K19*)] were significantly decreased in *Id2$^{-/-}$* MECs compared with those of controls, whereas the expression

levels of basal and/or myoepithelial markers [i.e. smooth muscle actin (*Sma*) and cytokeratin 14 (*K14*)] were comparable (Fig. 2B,C). A recent study revealed that luminal cells comprise K8^{high} and K8^{low} cells (Davis et al., 2016). To examine whether *Id2$^{-/-}$* mice have either a reduced luminal population or only few K8^{high} cells with intact number of luminal cells, we performed immunohistochemistry (IHC) for E-cadherin (cadherin 1; E-cad), K8 and K14. Quantification data for IHC and immunoblotting data showed that *Id2$^{-/-}$* mice had a decreased number of both E-cad$^+$ luminal cells (0.79-fold) and K8^{high} cells (0.54-fold) (Fig. 2D-M), indicating that deletion of ID2 resulted in the reduction of all luminal cell types, including K8^{high} cells. Constantly, immunoblotting showed decreased expression of E-cad and K8 but not of SMA in *Id2$^{-/-}$* MECs (Fig. 2H), suggesting that ID2 has important roles in luminal lineage cells.

Id2$^{-/-}$ mice showed side-branching defects but had normal TEBs and primary ducts, suggesting that primary ducts of *Id2$^{-/-}$* mice have a cell composition similar to wild-type mice, but with a reduced number of luminal cells in putative side-branch points. Given that most side branches are found in proximal rather than distal regions (Šale et al., 2013), we divided the inguinal mammary glands of *Id2$^{-/-}$* mice into proximal and distal regions, and performed IHC for K8 and SMA. We found that numerous *Id2$^{-/-}$* ducts in the distal region showed an intact cell composition or a mild reduction of K8$^+$ cells, whereas many *Id2$^{-/-}$* ducts in the proximal region showed a severe reduction in K8$^+$ cells (Fig. 2G-L). These results suggest that side-branching defects in *Id2$^{-/-}$* mice are caused by impaired luminal lineage differentiation.

To further investigate which luminal cells are affected in *Id2$^{-/-}$* mice, we performed flow cytometry analysis. In *Id2$^{-/-}$* mice, CD29^{mid}CD24^{high} luminal cells (Shackleton et al., 2006) were significantly reduced compared with controls, whereas the population of CD29^{high}CD24$^+$ basal and/or myoepithelial cells was increased, which could be explained by the decreased number of luminal cells. Interestingly, among the CD29^{mid}CD24^{high} luminal cells, CD61$^+$ LPs (Asselin-Labat et al., 2007) were markedly decreased in *Id2$^{-/-}$* mice compared with controls (0.21-fold) (Fig. 2O,P). qRT-PCR and immunoblotting analysis also showed decreased CD61 expression in *Id2$^{-/-}$* MECs compared with controls (Fig. 2N,Q). Taken together, our data suggested that ID2 is required for luminal lineage differentiation and generation of CD61$^+$ LPs.

Budding and side branch-specific CD61 expression

Based on side-branching defects and decreased CD61$^+$ LPs in *Id2$^{-/-}$* mice, we investigated whether CD61$^+$ LPs are involved in side branching. Using traditional methods for mammary tissue preparation, it was difficult to discriminate the side branches from a tilted cut of primary ducts in the cross-section of mammary tissues. To overcome this limitation, we developed a flattened tissue preparation method by dehydrating mammary tissues (see also Materials and Methods). Through the improved tissue preparation method, side and budding branches were distinguishable and morphologically distinct from one another. Surprisingly, in the IHC analysis, CD61 was highly expressed in budding and side branches, but rarely expressed in primary ducts (Fig. 3A-D).

To prove that CD61$^+$ LPs reside in side branches, we performed 3D mammary tissue imaging using the clear, unobstructed brain imaging cocktails and computational analysis (CUBIC) method (Lloyd-Lewis et al., 2016; Susaki et al., 2014). Our 3D imaging data clearly showed that CD61 was dominantly expressed in laterally budding branches rather than in primary ducts, whereas K8 was ubiquitously expressed both in primary ducts and side branches (Fig. 3E,F and Movies 1 and 2). Co-staining of CD61 with
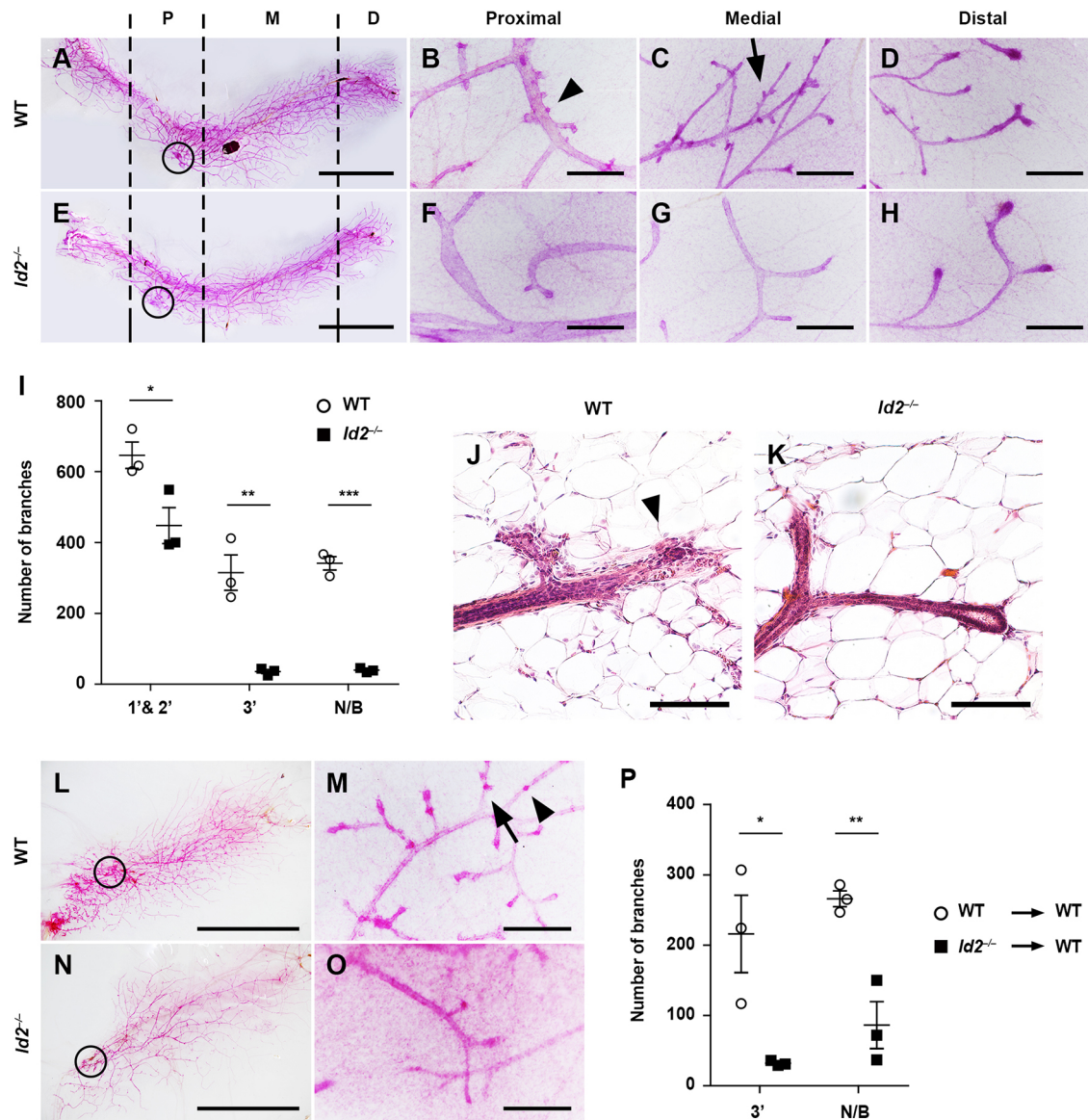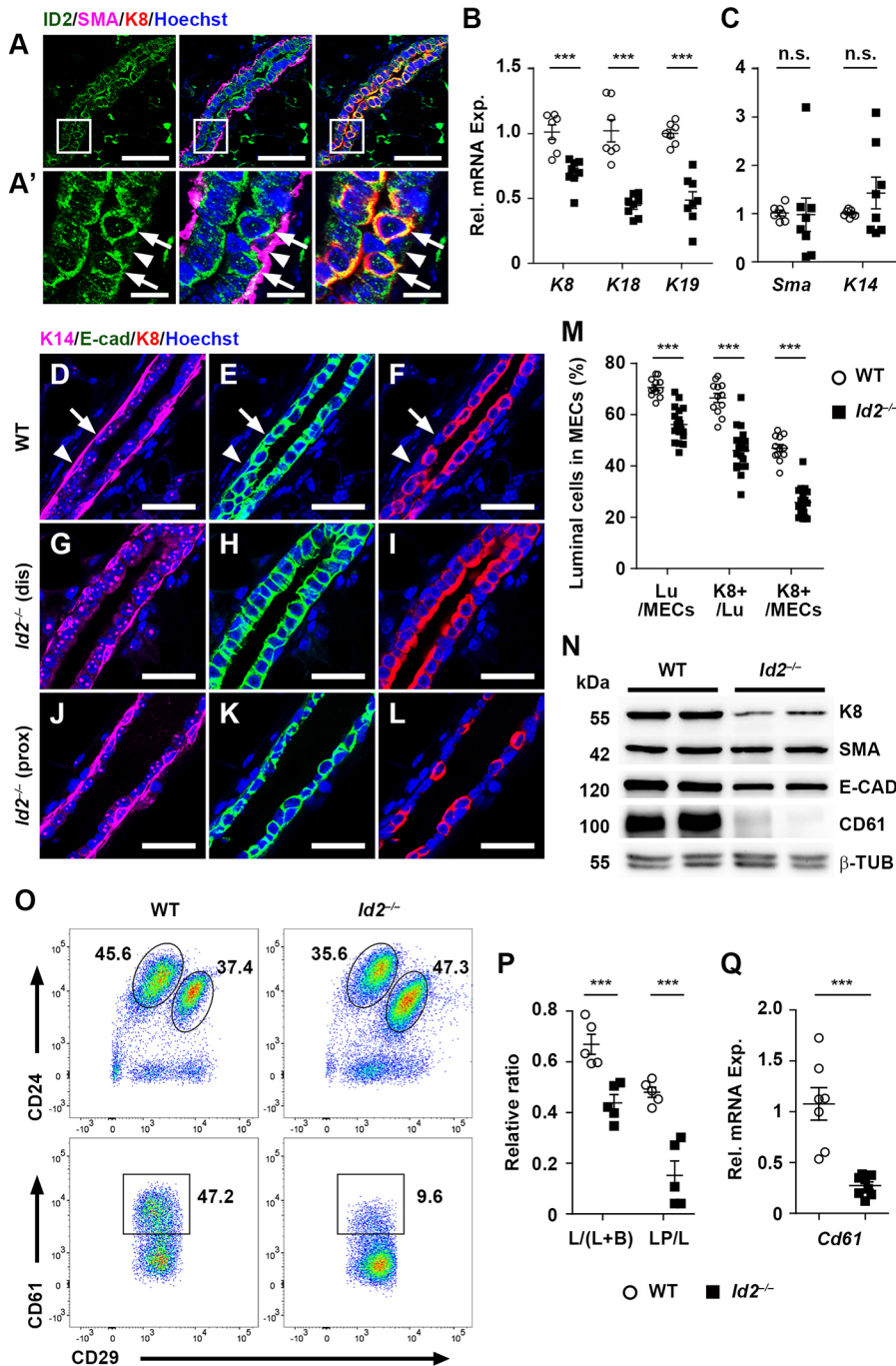
Fig. 1. Cell-autonomous side-branching defects in *Id2*^{−/−} virgin mice. (A-I) C-A-stained mammary glands (A-H) and quantification of branches (I) in 8-week-old wild-type and *Id2*^{−/−} mice. *Id2*^{−/−} mice showed intact TEBs and fat-pad coverage of primary ducts. However, side and nascent and/or budding branches were dramatically decreased in *Id2*^{−/−} mice. All mice were sacrificed at diestrus. The circle indicates the nipple, whereas the arrow indicates side branches and the arrowhead indicates nascent and/or budding side branches. 1′, 2′, 3′ and N/B represent the primary duct, secondary branch, tertiary branch (terminal side branch) and nascent and/or budding side branch, respectively. (J,K) H&E-stained mammary glands from 8-week-old wild-type and *Id2*^{−/−} mice. *Id2*^{−/−} mice showed intact end buds. Arrowhead indicates nascent and/or budding side branches. (L-P) C-A-stained mammary glands (L-O) and quantification of branches (P) from transplanted wild-type and *Id2*^{−/−} MECs. We used 8- and 3-week-old mice as donors and recipients, respectively. The number of tertiary side branches in *Id2*^{−/−} transplants was dramatically decreased compared with wild-type transplants, indicating that ID2 is required for side branching in a cell-intrinsic manner. The circle indicates the transplantation point in the cleared fat pads, whereas the arrow indicates side branches and the arrowhead indicates nascent and/or budding side branches. Scale bars: 1 cm in A,E,L,N; 1 mm in B-D,F-H; 100 μm in J,K; 0.5 mm in M,O. For all figures, *N*=3, each. Data are means±s.e.m., analyzed using Student's *t*-test: *$P<0.05$, **$P<0.01$ and ***$P<0.001$. Proximal (P), near the nipple; medial (M), near the lymph node; distal (D), outermost region. See also Fig. S1.

K8 showed that most CD61^{+} cells were negative for K8, although some CD61^{+} cells were K8^{+} (Fig. 3G). Given that K8^{high} cells are regarded as mature luminal cells with PGR expression (sensor cells) (Brisken, 2013; Brisken and Duss, 2007; Davis et al., 2016), CD61 and K8-double positive cells might be cells differentiating from CD61^{+} LPs into mature K8^{+} luminal cells or luminal lineage-determined progenitor cells.

TEBs have a characteristic structure with cap cells and multilayered body cells, in which stem and/or progenitor cells proliferate actively and differentiate into myoepithelial and luminal lineage cells (Gajewska et al., 2013; Scheele et al., 2017; Woodward et al., 2005). Given that CD61^{+} cells have progenitor characteristics, they might reside in TEBs as well as in side branches. To examine whether CD61^{+} LPs also reside in TEBs, we performed IHC on bromodeoxyuridine (BrdU)-incorporated tissues. Unexpectedly, CD61^{+} cells were barely detected in TEBs (Fig. 3H-J). Collectively, these findings indicate that CD61^{+} LPs reside in side branches but not in TEBs, suggesting that differentiation of CD61^{+} LPs is crucial for the formation of side branches but not for primary elongation.

Fig. 2. Reduction of luminal lineage cells in Id2⁻/⁻ mice. (A,A′) IHC analysis of ID2, K8 and SMA in 8-week-old virgin mammary glands. ID2 was detected exclusively in luminal cells. K8 and SMA represent luminal and basal and/or myoepithelial markers, respectively. Arrows indicate ID2$^+$K8$^+$ luminal cells and arrowhead indicates ID2$^-$SMA$^+$ myoepithelial cells. Images in A′ are magnifications of the boxed areas in A. (B,C) mRNA expression of luminal (*K8*, *K18* and *K19*)- and basal and/or myoepithelial (*Sma* and *K14*) cell markers in wild-type and *Id2*⁻/⁻ MECs. All gene expression levels were normalized to *Uxt* (ubiquitously expressed transcript protein; see also Materials and Methods). *n*=7 (wild type), *n*=8 (*Id2*⁻/⁻). (D-M) IHC staining for K8, E-cad, K14 (D-L) and quantification of E-cad$^+$ and K8$^+$ luminal cells in MECs (M) from 8-week-old wild-type and *Id2*⁻/⁻ mammary glands. *Id2*⁻/⁻ mice showed significantly reduced K8$^+$ and E-cad$^+$ luminal cells with intact K14$^+$ cells. Arrow indicates E-cad$^+$ K8$^-$ K14$^-$ luminal cells whereas arrowhead indicates E-cad$^-$ K8$^-$ K14$^+$ basal cells. Lu indicates E-cad$^+$ luminal cells, K8+ indicates K8$^+$ luminal cells and MECs represent the sum of K14$^+$ and E-cad$^+$ cells. *n*=4 (wild type), *n*=6 (*Id2*⁻/⁻). For statistics, we extracted three slides from each mouse. (N) Immunoblotting analysis of isolated wild-type and *Id2*⁻/⁻ MECs. (O) Flow cytometric analysis of CD29^{mid}CD24^{high} luminal, CD29^{high}CD24$^+$ basal and/or myoepithelial and CD29^{mid}CD24^{high}CD61$^+$ LP populations. The CD29-CD61 plot was generated from the CD29^{mid}CD24^{high} luminal population. Luminal cells, particularly CD61$^+$ LPs, were dramatically decreased in *Id2*⁻/⁻ mice. (P) Proportion of the luminal population in whole MECs and LP populations in the luminal population based on flow cytometry data. *n*=5 (wild type), *n*=5 (*Id2*⁻/⁻). (Q) *Cd61* mRNA expression in wild-type and *Id2*⁻/⁻ MECs. *n*=7 (wild type), *n*=8 (*Id2*⁻/⁻). For all figures, Data are means±s.e.m., analyzed by Student's *t*-test: ****P*<0.001. Scale bars: 50 μm in A; 10 μm in A′; 30 μm in D-L. β-TUB, β-tubulin; L, luminal; B, basal/myoepithelial cells.

Accumulation of aberrant K6⁺ BPs in Id2⁻/⁻ mice

Given that CD61$^+$ LPs have been suggested as progenitor cells (Asselin-Labat et al., 2007), decreased CD61$^+$ LPs in *Id2*⁻/⁻ mice could result from the impaired proliferation of CD61$^+$ LPs. To address this possibility, we performed a BrdU incorporation assay. In contrast to expectations, most CD61$^+$ cells in the side branches were BrdU negative (Fig. 3J) even in wild-type mice, suggesting that the reduction of CD61$^+$ LPs in *Id2*⁻/⁻ mice is not caused by their proliferation defects. To further investigate whether decreased CD61$^+$ LPs in *Id2*⁻/⁻ mice were caused by developmental blockage of primitive stem and/or progenitor cells into CD61$^+$ LPs, we examined the expression of K6, a putative marker of BPs (Bu et al., 2011; Grimm et al., 2006; Smith et al., 1990; Sun et al., 2010). K6$^+$ cells were observed in a few ducts of 8-week-old wild-type mice

(Fig. 4A-D,I). Intriguingly, a considerable number of *Id2*⁻/⁻ ducts showed markedly increased numbers of K6$^+$ cells with dramatically reduced K8$^+$ mature luminal cells (Fig. 4E-I). Consistent with these findings, qRT-PCR and immunoblotting analyses also showed increased K6 expression in *Id2*⁻/⁻ mice compared with controls (Fig. S2A,B).

To investigate the blockage of K6$^+$ BPs developing into CD61$^+$ LPs in *Id2*⁻/⁻ mice, we performed flow cytometry analysis using CD49b (integrin-α2), a promising LP marker (Shehata et al., 2012), along with CD61, and revealed that most CD61$^+$ cells were CD49b$^+$ (98.44±0.44%), whereas ~30.40±2.29% CD49b$^+$ cells were CD61$^-$. These data suggest that there are two distinct subsets of LPs, namely CD61$^+$CD49b$^+$ and CD61$^-$CD49b$^+$ LPs, in the CD29^{mid}CD24^{high} luminal cell population. CD61$^+$CD49b$^+$ LPs were dramatically
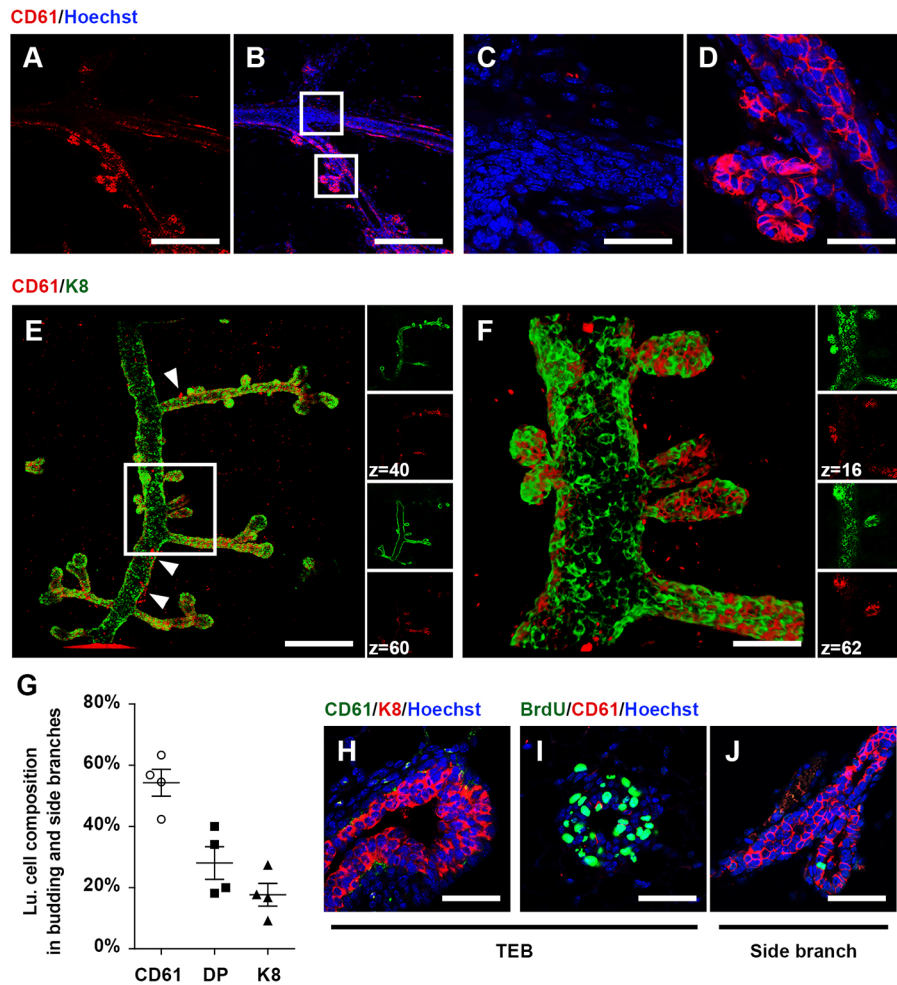
Fig. 3. CD61 expression specifically in budding and side branches. (A-D) IHC staining for CD61 of flattened mammary gland tissues from 8-week-old wild-type mice. (E,F) CUBIC clearing and 3D imaging of 8-week-old wild-type mammary glands. The images were reconstituted with 125 Z-stacks (1 μm-interval). CD61 was dominantly detected in side and budding branches but barely in primary ducts. Arrowhead indicates nonspecific signals based on a rotated view (Movies 1 and 2). (G) Cell composition of luminal cells in budding and side branches. For statistics, we observed 14 budding and side branches from three mice. CD61 indicates CD61$^+$K8$^-$ cells, K8 indicates CD61$^-$K8$^+$ cells and DP indicates CD61 and K8 double-positive cells. Data are means±s.e.m. (H-J) IHC staining for CD61, K8 and BrdU. Terminal end buds were highly proliferative (I) and comprised multilayered body cells (H). CD61 was barely detected in TEBs, whereas numerous CD61$^+$ cells with few BrdU$^+$ cells were detected in side branches (J). Only 1.91%±1.41% (mean±s.e.m.) of CD61$^+$ cells were BrdU positive. Scale bars: 200 μm in A,B,E; 50 μm in F,H-J; 40 μm in C,D. See also Movies 1 and 2.

decreased in $Id2^{-/-}$ mice compared with controls, whereas the CD61$^-$CD49b$^-$ population increased (Fig. 4J), which might be because of increased K6$^+$ BPs in $Id2^{-/-}$ mice. To address this issue, we sorted CD61$^-$CD49b$^-$ cells and CD61$^+$CD49b$^+$ cells from CD29^{mid}CD24^{high} luminal cells and immunostained them with anti-K6 antibody. As expected, K6$^+$ BPs were enriched in the CD61$^-$CD49b$^-$ population (Fig. 4K,L), and qRT-PCR data also showed increased $K6$ expression in the CD61$^-$CD49b$^-$ population (Fig. S2C). Consistent with immunohistochemical analysis (Fig. 4A-I), the number of K6$^+$ cells was greatly increased in the CD61$^-$CD49b$^-$ population from 6-week-old $Id2^{-/-}$ mice compared with controls (Fig. 4M,N and Fig. S2D). K6$^+$ BPs are abundant at 4-6 weeks of age, gradually decrease with age and finally disappear after 12 weeks of age (Sun et al., 2010). Intriguingly, abundant K6$^+$ cells were still detected even in 14-month-old $Id2^{-/-}$ mice, but were rarely detected in controls of the same age (Fig. 4M,N).

To further examine whether the increase of K6$^+$ BPs in $Id2^{-/-}$ ducts results from the continuous proliferation of K6$^+$ BPs, we conducted IHC for proliferating cell nuclear antigen (PCNA) and K6. Unexpectedly, however, most K6$^+$ cells in $Id2^{-/-}$ mice were PCNA negative, whereas control mice were PCNA positive (Fig. 4O,P). Consistently, cyclin-dependent kinase inhibitor 1B (CDKN1B or p27) was expressed in K6$^+$ cells of $Id2^{-/-}$ ducts, but not in controls (Fig. S2E). When we examined the expression levels of the CDK inhibitors $p15$, $p16$, $p21$ and $p27$ in the K6$^+$ BP-enriched CD61$^-$CD49b$^-$ cells, their expression was dramatically increased in $Id2^{-/-}$ K6$^+$ BP-enriched CD61$^-$CD49b$^-$ cells compared with controls

(Fig. 4Q). Taken together, $Id2^{-/-}$ mice had accumulated aberrant K6$^+$ BPs, indicating that disruption of ID2 blocks the differentiation of K6$^+$ BPs into CD61$^+$CD49b$^+$ (hereafter CD61$^+$, given that most of the CD61$^+$ cells were CD49b$^+$) LPs.

Differentiation of K6$^+$ BPs into CD61$^+$ LPs and side-branch formation by nuclear ID2

To examine whether ID2 induces the differentiation of K6$^+$ BPs into CD61$^+$ LPs, we transfected either HA-tagged $Id2$ or HA-NLS-tagged $Id2$ genes into HC11 cells, and conducted immunocytochemistry (ICC) analysis for HA and either K6 or CD61. Notably, the ectopic expression of NLS-$Id2$ into HC11 cells resulted in the induction of CD61$^+$ cells but showed a significant reduction of K6$^+$ cell numbers compared with cells overexpressing $Id2$ (Fig. 5A-C and Fig. S3A-C), in which the cells with cytosolic ID2 remained as K6$^+$ and CD61$^-$ (arrowhead in Fig. 5A,B and Fig. 3A-C), whereas the cells with nuclear ID2 resulted in K6$^-$ and CD61$^+$ (arrow in Fig. 5A,B and Fig. 3A-C). Even in HA-$Id2$ vector-transfected groups, the cells with nuclear ID2 were CD61-positive (Fig. 5A and Fig. S3A-C). Consistently, overexpression studies using human mammary cell lines (MCF10A, MCF7, SK-BR3, HCC70 and AU565) also showed similar results (data not shown). Collectively, our data showed that ID2, particularly nuclear ID2, strongly drives the differentiation of K6$^+$ BPs into CD61$^+$ LPs.

Next, to examine whether nuclear translocation of ID2 is crucial for side branching, we generated and examined NLS-$Id2$ Tg mice. NLS-$Id2$ Tg mice showed a 3.2-fold and 9.2-fold increase in the
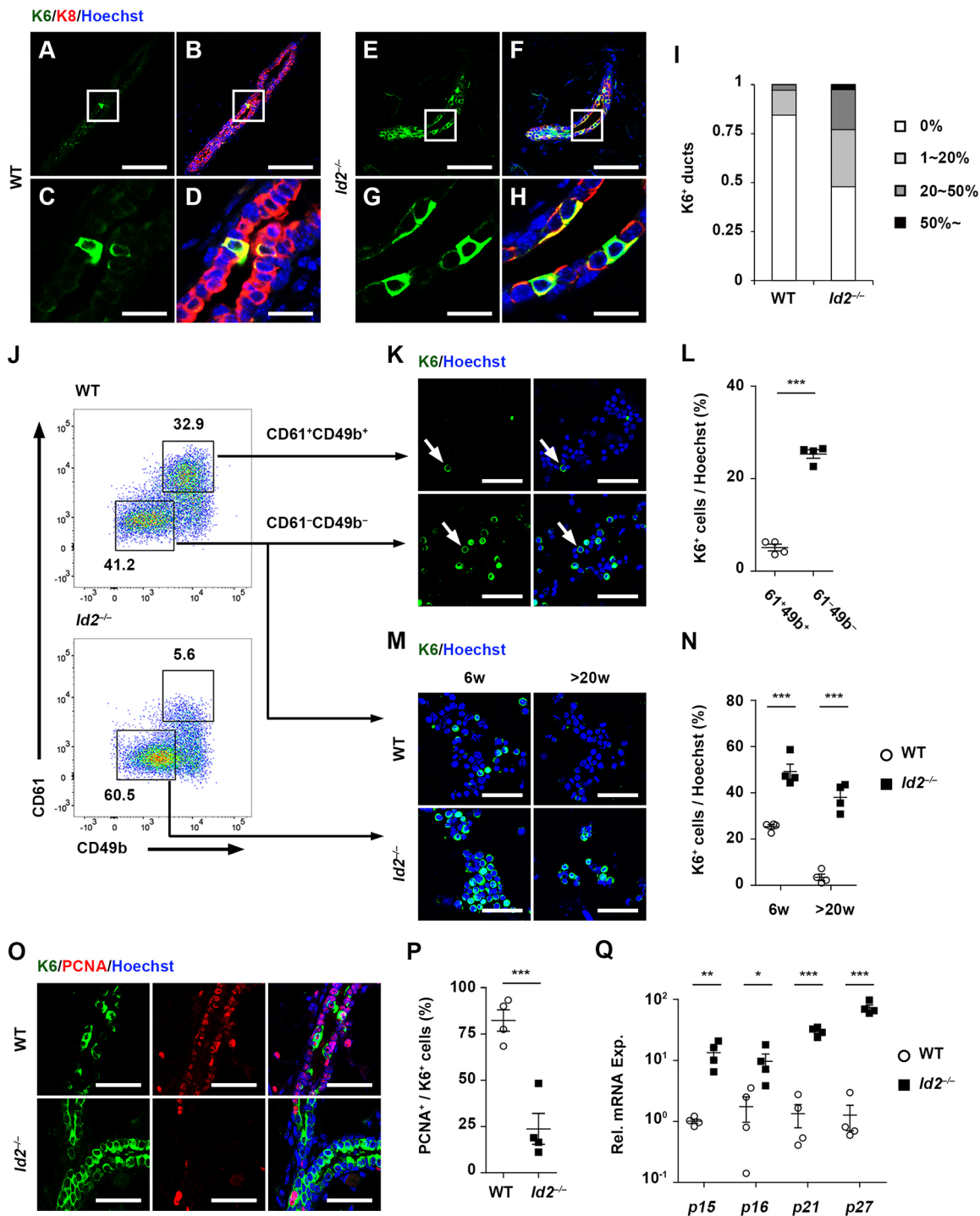
Fig. 4. Accumulation of aberrant K6$^+$ BPs by deletion of ID2. (A-I) IHC staining for K6 and K8 in 8-week-old wild-type (A-D) and $Id2^{-/-}$ (E-H) mice, and quantification of ducts according to the proportion of K6$^+$ cells in Hoechst-stained luminal cells (I). Most wild-type ducts had no K6$^+$ cells (120/142), but over half of $Id2^{-/-}$ ducts (107/205) had K6$^+$ cells. For quantification, we used two sides from each of three mice. (J) Schematic view of CD61$^+$CD49b$^+$ and CD61$^-$CD49b$^-$ population sorting with 6-week-old wild-type and $Id2^{-/-}$ mice. The plot was generated from the CD29^{mid}CD24^{high} luminal population. (K,L) ICC analysis for K6 with CD61$^+$CD49b$^+$ and CD61$^-$CD49b$^-$ luminal cells from 6-week-old wild-type mice (K), and proportion of K6$^+$ cells in each population (L). Most K6$^+$ cells were found in CD61$^-$CD49b$^-$ luminal cells. Arrow indicates K6$^+$ cells with minimum fluorescence intensity. (M,N) ICC staining for K6 with CD61$^-$CD49b$^-$ luminal cells from 6- or >20-week-old wild-type and $Id2^{-/-}$ mice (M), and proportion of K6$^+$ cells in each population (N). Whereas matured wild-type mice barely had any K6$^+$ cells, old $Id2^{-/-}$ mice contained numerous K6$^+$ cells. We detected K6$^+$ cells even in 14 months of age $Id2^{-/-}$ mice. (O,P) IHC staining for K6 and PCNA of flattened mammary gland tissues from 6-week-old wild-type and $Id2^{-/-}$ mice (O), and quantification of PCNA$^+$ cells in K6$^+$ cells (P). To secure enough K6$^+$ cells, we used 6-week-old mice rather than 8-week-old mice for the K6 studies. Although K6 represents BPs, K6$^+$ cells in $Id2^{-/-}$ mice were not proliferative, whereas most of the K6$^+$ cells in wild-type mice had entered the cell cycle. (Q) qRT-PCR for cell cycle inhibitors with CD61$^-$CD49b$^-$ luminal cells from 6-week-old wild-type and $Id2^{-/-}$ mice. Dramatic increase of K6$^+$ BPs without cell proliferation in $Id2^{-/-}$ mice indicates that ID2 is crucial for the differentiation of K6$^+$ BPs into CD61$^+$ LPs. For each figure, n=4 each; data are means±s.e.m., analyzed by Student's t-test: *P<0.05, **P<0.01, ***P<0.001. Scale bars: 100 μm in A,B,E,F; 30 μm in K,M; 20 μm in C,D,G,H,O. See also Fig. S2.
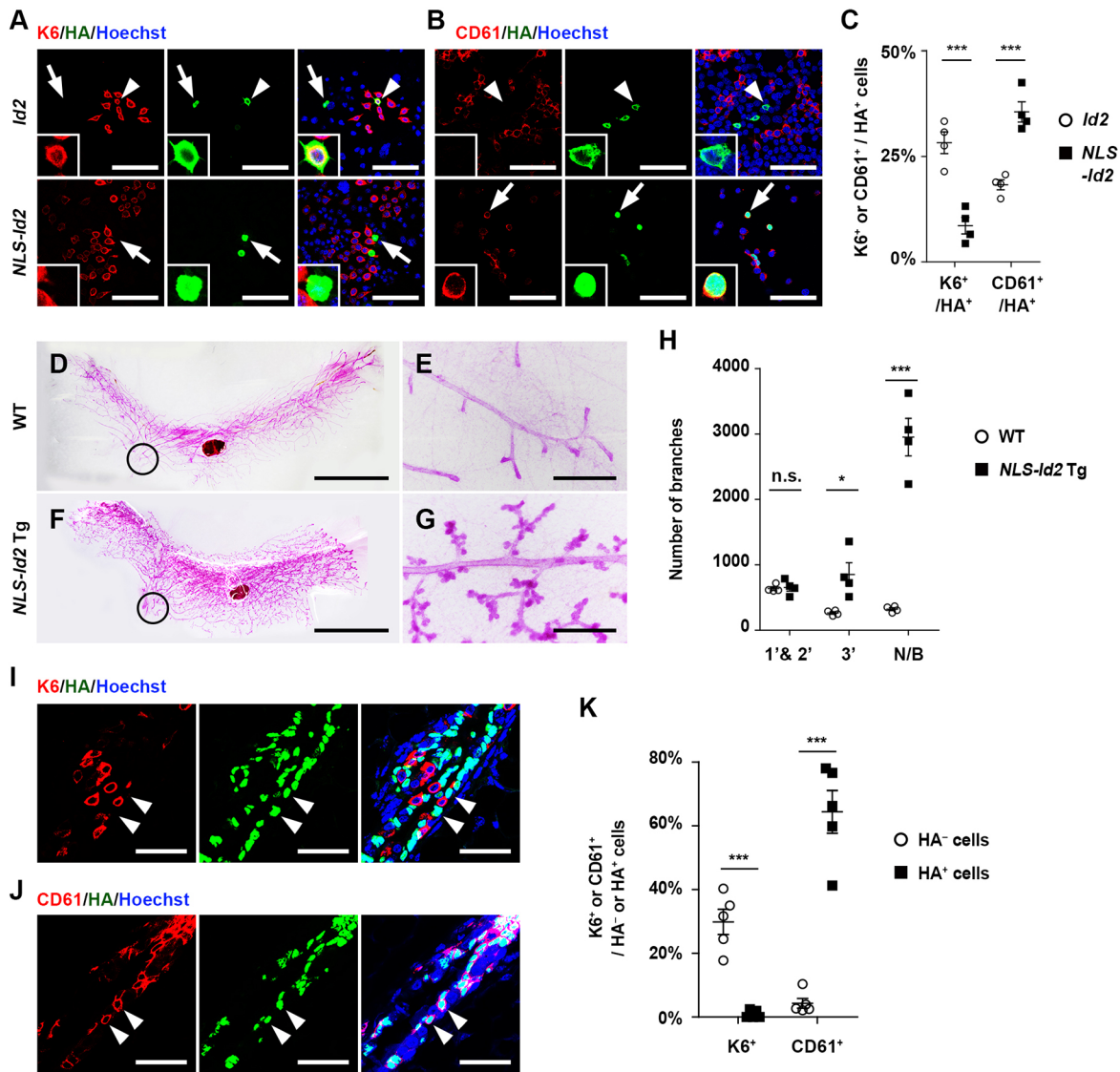
Fig. 5. Induction of side branching and luminal lineage differentiation by nuclear ID2. (A-C) ICC staining for CD61, K6 and HA in HC11 cells transfected with HA-tagged *Id2*- or HA-tagged *NLS-Id2*-overexpressing vectors (A,B), and quantification of K6$^+$ or CD61$^+$ cells in HA-positive HC11 cells (C). The cells with nuclear ID2 showed significant reduction of K6 and induction of CD61 expression. HA$^-$CD61$^+$ cells might be CD61$^+$ cells that were differentiated by endogenous ID2 rather than ectopic ID2. Arrow indicates nuclear ID2 and the arrowhead indicates cytosolic ID2. n=4, each. For statistics, we counted at least 100 HA$^+$ cells for each set of data. (D-H) C-A-stained inguinal mammary glands (D-G) and quantification of branches (H) in 8-week-old wild-type and *NLS-Id2* Tg mice. Overexpression of nuclear ID2 resulted in dramatic increase of side branches and nascent and/or budding branches. The circle indicates the nipple. 1′, 2′, 3′ and N/B represent the primary duct, secondary branch, tertiary branch (terminal side branch) and nascent and/or budding branch, respectively. n=4, each. (I-K) IHC staining for HA, and either K6 or CD61 in 8-week-old *NLS-Id2* Tg mice (I,J) and quantification of K6$^+$ or CD61$^+$ cells in HA$^+$ cells (K). Luminal cells having nuclear ID2 did not express K6 (K6$^+$/nuclear ID2$^+$ cells, 0.00%; K6$^+$/whole luminal cells, 4.48%±1.69%) but did express CD61, suggesting that ID2 strongly differentiates K6$^+$ BPs into CD61$^+$ LPs. Arrowhead indicates HA$^+$ cells. n=5, each. For each figure, data are means±s.e.m. analyzed by Student's *t*-test: ***P<0.001. Scale bars: 100 μm in A,B; 20 μm in I,J; 1 cm in D,F; 1 mm in E,G. See also Fig. S3.

number of nascent and/or budding and side branches compared with controls, respectively (Fig. 5D-H). Intriguingly, although there was no difference in the numbers of primary and secondary ducts, *NLS-Id2* Tg mice showed slightly delayed primary ductal elongation, which might be because of diverted resources being used for drastic side-branching induction. Indeed, 10-week-old *NLS-Id2* Tg mice showed primary ducts of normal length, similar to those of control mice (data not shown).

To investigate whether nuclear ID2 induces the differentiation of K6$^+$ BPs into CD61$^+$ LPs *in vivo*, we conducted IHC for HA, and either K6 or CD61, using *NLS-Id2* Tg mice. Notably, almost all HA$^+$ cells (the cells with overexpressed nuclear ID2) were K6$^-$ but

CD61$^+$, consistent with *in vitro* data (Fig. 5I-K). Moreover, CD61$^+$ cells were observed at budding and side branches in *NLS-Id2* Tg mice similar to those of wild-type mice (Fig. S3D-G).

H&E staining showed that *NLS-Id2* Tg mice appeared to have alveolus-like structures, even in virgin mice (Fig. S3H). To elucidate the characteristics of alveolus-like structures in *NLS-Id2* Tg mice, we examined the gene expression profiles of typical milk protein genes, such as β-casein (*Csn2*), whey acidic protein (*Wap*) and α-lactalbumin (*Lalba*). However, there was no significant induction of milk protein genes in *NLS-Id2* Tg mice compared with wild-type virgin mice (Fig. S3I). Moreover, alveolus-like structures in *NLS-Id2* Tg mice had shapes that were obviously different compared with the

alveoli of lactation day 1 (L1) mice (Fig. S3J-L), indicating that alveolus-like structures in *NLS-Id2* Tg mice are budding branches rather than milk-producing lobuloalveoli. Taken together, our findings showed that *NLS-Id2* Tg mice had dramatically increased nascent and/or budding and side branches, and that nuclear ID2 induced the luminal lineage commitment and formation of nascent and/or budding branches.

Nuclear ID2 as a key mediator of progesterone for side branching and differentiation into CD61^{+} LPs

We previously reported that RANKL, a key mediator of progesterone signaling, induced nuclear retention of ID2 in lactating mammary glands (Kim et al., 2006, 2011), suggesting that ID2 nuclear localization is induced by progesterone signaling. To investigate whether nuclear ID2 acts as a key mediator of progesterone for side branching, we performed Ovx in 5-week-old wild-type and *NLS-Id2* Tg mice, and administered 17β-estradiol with or without progesterone (Fig. S4A). We also prepared corn oil-administered Ovx groups as negative controls (Fig. 6A,D). Estradiol alone barely induced side branching in wild-type Ovx mice, whereas administration of 17β-estradiol with progesterone induced the formation of normal ductal trees (Fig. 6B,C). Notably, in *NLS-Id2* Tg Ovx mice, 17β-estradiol alone readily induced side branches, which were comparable to those in wild-type Ovx mice treated with both 17β-estradiol and progesterone (Fig. 6E,G). The administration of both 17β-estradiol and progesterone to *NLS-Id2* Tg Ovx mice resulted in comparable numbers of nascent and/or budding branches and side branches compared with those of 17β-estradiol alone (Fig. 6F), indicating that overexpression of nuclear ID2 can replace the function of progesterone. To demonstrate the overexpression of nuclear ID2 in *NLS-Id2* Tg Ovx mice treated with 17β-estradiol, we conducted IHC for HA with *NLS-Id2* Tg sham and Ovx mice administered with corn oil, 17β-estradiol, and both 17β-estradiol and progesterone. We found that nuclear ID2 was overexpressed in all hormone-treated groups (Fig. S4C-G). Taken together, our results showed that nuclear ID2 is a key mediator of progesterone signaling, which induces new side branches.

Progesterone is essential for the terminal differentiation of luminal cells (Beleut et al., 2010; Lee et al., 2013) as well as side branching. To investigate whether nuclear ID2 also has a role in luminal differentiation as a mediator of progesterone signaling, we performed Ovx in 3-week-old wild-type and *NLS-Id2* Tg mice and administered 17β-estradiol with or without progesterone (Fig. S4B). Wild-type Ovx mice treated with 17β-estradiol showed decreased populations of CD29[mid]CD24^{high} luminal cells and CD61^{+} LPs compared with sham groups, and wild-type Ovx mice treated with both 17β-estradiol and progesterone rescued the impaired luminal lineage differentiation (Fig. 6H), indicating that progesterone induces luminal lineage differentiation. Importantly, in *NLS-Id2* Tg Ovx mice, 17β-estradiol alone substantially induced the differentiation of luminal lineage cells, comparable with sham groups (Fig. 6H and Fig. S4H). These data indicated that nuclear ID2 overexpression is sufficient to induce luminal lineage differentiation, even without progesterone.

To confirm whether ID2 is a mediator of progesterone signaling in the differentiation of luminal lineage cells, we conducted flow cytometry with *Id2*^{−/−} Ovx mice after treatment with 17β-estradiol alone or with both 17β-estradiol and progesterone. Both groups of *Id2*^{−/−} Ovx mice showed impaired CD29[mid]CD24^{high} luminal and CD61^{+} LP populations (Fig. S4I). Progesterone barely induced the differentiation of CD61^{+} LPs without ID2, indicating that ID2 is a key mediator of progesterone signaling for luminal lineage differentiation.

Failure of CD61^{+} LP-derived tumor formation in *Id2*^{−/−} mice

The *MMTV-active Neu* Tg (*Neu* Tg) mouse is a model widely used for investigating LP-derived tumors (Lo et al., 2012; Prat and Perou, 2009; Vaillant et al., 2008). As reported, tumor tissues (T) in *Neu* Tg mice (*Neu*_T) displayed high levels of *K8* and *Cd61*, but almost no *K14* (Vaillant et al., 2008) (Fig. S5A-D). Flow cytometry analysis also revealed that tumor tissues comprised CD61^{+} LPs (Fig. 7A). Along with increased *Cd61* expression, the dramatically decreased *K6a* expression (Fig. S5E) indicated that NEU strongly drives the differentiation of K6^{+} BPs into CD61^{+} LPs.

To prove that ID2 induces the generation of functional CD61^{+} LPs rather than merely *Cd61* expression, we crossed *Id2*^{−/−} mice with *Neu* Tg mice and hypothesized that LP-derived tumors will not be established in *Neu* Tg;*Id2*^{−/−} mice if there was no cellular source for tumor occurrence. Importantly, we could not find any sign of tumors in *Neu* Tg;*Id2*^{−/−} mice until they were 70 weeks old, whereas all *Neu* Tg and *Neu* Tg;*Id2*^{+/−} mice developed CD61^{+} LP-derived tumors before they were 55 weeks old (Fig. 7D). C-A staining also showed no occurrence of microtumors or even foci in *Neu* Tg;*Id2*^{−/−} mice (Fig. 7E-J). Flow cytometry analysis showed markedly decreased populations of CD29[mid]CD24^{high} luminal cells and CD61^{+} LPs in *Neu* Tg;*Id2*^{−/−} mice, despite intact expression of *Neu* (Fig. 7C and Fig. S5F). qRT-PCR and western blotting also showed that the expression levels of CD61, K8 and K18 were decreased in *Neu* Tg; *Id2*^{−/−} mice compared with those in non-tumor tissues (NT) from *Neu* Tg mice (*Neu*_NT), whereas K6 was increased (Fig. 7K-O). *Neu* Tg;*Id2*^{−/−} mice did not show any decrease in NEU target genes, indicating that loss of ID2 does not affect canonical NEU signaling (Fig. S5G). Collectively, without ID2, NEU barely drove the differentiation of K6^{+} BPs into CD61^{+} LPs and could not induce LP-derived tumors, indicating that ID2 is essential for the differentiation of K6^{+} BPs into functional CD61^{+} LPs (Fig. 8A,B).

DISCUSSION

Mammary glands are essential for nursing offspring in mammals. To produce a sufficient amount of milk, mammary glands overcome the spatial restriction of mammary epithelium in fat pads through side branching, similar to the trees of the trachea in the lung. Previous studies revealed that ID2 is necessary for proper lobuloalveologenesis during pregnancy, but the target cells and mechanism of action of ID2 have remained unsolved. In this study, we found that ID2 is crucial for side branching but not for primary ductal elongation, and that nuclear ID2 strongly drives the differentiation of K6^{+} BPs into CD61^{+} LPs in budding side branches. Importantly, ovariectomy and hormone reconstitution studies revealed that nuclear ID2 drives side branching and luminal differentiation even without progesterone. Taken together, our findings suggest that ID2, as a mediator of progesterone, regulates side branching by inducing the differentiation of CD61^{+} LPs at putative side-branching points.

Recently, using *Rosa-confetti* mice, Scheele et al. reported that the bifurcation of TEBs is determined probabilistically (Scheele et al., 2017) and that branching occurs nearly exclusively through TEB bifurcation but not through side branching. Their observations were based on comparison of the branch length distributions between ductal trees of 5-week-old and 8-week-old mice and the results of an EdU incorporation assay, in which proliferation activity was detected in TEBs but not in existing ducts. The same group also reported the mechanism of ductal morphogenesis using the same model, in which EdU-positive signals were detected even in existing ducts of the proximal region near the nipple (Hannezo et al., 2017), suggesting that *de novo* side branching occurs independently from
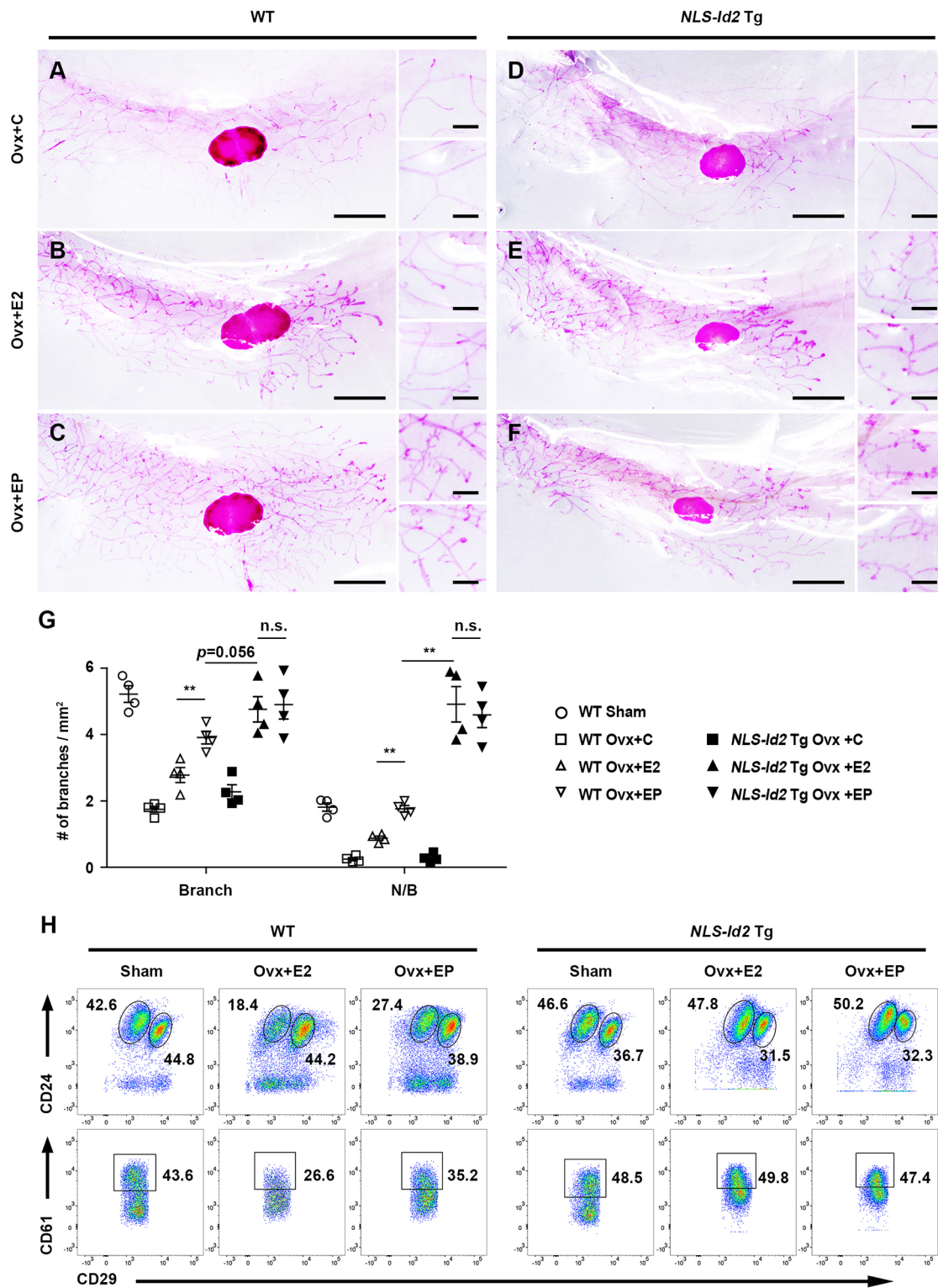
Fig. 6. See next page for legend.

the bifurcation of TEBs. Indeed, many studies reported the existence of side branching. When primary ducts reach the end of the fat pad, TEBs terminate proliferation and lose their structure. However, upon pregnancy, numerous side branches occur at the existing ducts (Brisken, 2013). Furthermore, progesterone administration to adult female mice results in an increase in side branches without the induction of primary elongation or bifurcation of TEBs (Atwood

et al., 2000). Šale et al. reported that tertiary side branches were detected in the proximal region but not in the distal region (Šale et al., 2013). Recently, the Visvader group also reported that putative MaSCs reside mainly in the proximal region rather than in TEBs (Fu et al., 2017), suggesting the existence of stem and/or progenitor cells in the proximal region for side branches. Although Scheele et al. clearly demonstrated how bifurcation of TEB occurs to form primary

Fig. 6. Nuclear ID2 as a key mediator of progesterone signaling for side branching and luminal lineage differentiation. (A-F) C-A-stained inguinal mammary glands from ovariectomized 5-week-old wild-type and *NLS-Id2* Tg Ovx mice treated with corn oil (C), 17β-estradiol (E2) and progesterone (P). Both negative control groups showed shrunk TEBs and rare side branches. Wild-type Ovx mice treated with 17β-estradiol alone had only a few side branches, whereas wild-type Ovx mice treated with both 17β-estradiol and progesterone (EP) showed considerable nascent and/or budding (N/B) and side branches. Importantly, *NLS-Id2* Tg Ovx mice treated with 17β-estradiol alone showed numerous side branches. (G) Numbers of branches in wild-type and *NLS-Id2* Tg Ovx mice based on C-A staining (Fig. 6A-F). Wild-type sham mice were additionally analyzed as a control. *n*=4, each. Data are means±s.e.m.; two-way ANOVA analysis and Student's *t*-tests. **$P<0.01$. (H) Flow cytometric analysis of $CD29^{mid}CD24^{high}$ luminal population upon hormone administration. The CD29-CD61 plot was generated from the $CD29^{mid}CD24^{high}$ luminal population. When given only 17β-estradiol, *NLS-Id2* Tg Ovx mice showed normal differentiation of luminal lineage cells, whereas wild-type Ovx mice showed reduced $CD29^{mid}CD24^{high}$ luminal and $CD61^+$ LP populations. In wild-type Ovx mice, 17β-estradiol and progesterone co-administration could not rescue luminal lineage differentiation completely, possibly because of an imbalance between ectopic 17β-estradiol and progesterone, unlike normal physiological conditions. Scale bars: 5 mm in A-F, 0.5 mm in the enlargements in A-F; See also Fig. S4.

and secondary ducts, the mechanism by which side branches are formed still needs to be investigated. Here, we report how side branches occur independently from primary ductal elongation.

Progesterone induces side-branch formation by secreting paracrine mediators, such as RANKL, to neighboring $RANK^+$ cells (Beleut et al., 2010; Fernandez-Valdivia et al., 2009; Grimm et al., 2016; Lee et al., 2013; Mukherjee et al., 2010; Obr et al., 2013; Rajaram et al., 2015), suggesting that PGR^+ cells are located near putative side-branch points. However, PGR is not specifically detected in budding branches but is widely distributed throughout ducts (Rajaram et al., 2015; Davis et al., 2016) (data not shown). Therefore, identifying the characteristics of $RANK^+$ cells could provide clues to elucidate the mechanism by which progesterone elicits side branching. In this study, we suggested that nuclear ID2 in $K6^+$ BPs is crucial for side branching and luminal lineage differentiation, and previously reported that ID2 nuclear translocation occurs in $RANK^+$ cells (Kim et al., 2006, 2011), indicating that $K6^+$ BPs in ducts would be a strong $RANK^+$ cell candidates in pubertal mammary gland development. Thus, side-branch formation might require both progesterone-sensing PGR^+ luminal cells and adjacent $K6^+$ BPs in ducts.

$K6^+$ BPs reside in TEBs and leave their progeny on ducts during ductal elongation (Grimm et al., 2006). Thus, the nuclear translocation of ID2 in remaining $K6^+$ BPs on primary ducts could induce side branching. Intriguingly, primary ducts and TEBs have $K6^+$ cells and $K8^+$ luminal cells (Smith et al., 1990; Sun et al., 2010) but few $CD61^+$ LPs, indicating that there is a $CD61^+$ LP-independent luminal differentiation pathway in TEBs. $K6^+$ BPs in TEBs appear to differentiate into mature luminal cells through $CD61^-$ LPs, whereas $K6^+$ BPs remaining in the middle of ducts differentiate into $CD61^+$ LPs by progesterone-mediated nuclear translocation of ID2 to form side branches. This can explain why $Id2^{-/-}$ mice showed severe defects in side branching but exhibited normal TEBs despite having few $CD61^+$ LPs. Collectively, our findings suggest that nuclear ID2 induces side branching by promoting the differentiation of $K6^+$ BPs into $CD61^+$ LPs at putative side-branching points, and that a $CD61^+$ LP-independent luminal differentiation pathway is involved in primary ductal elongation.

Signal transducer and activator of transcription 5 (STAT5) is a well-known master regulator of alveologenesis and induces the differentiation of $CD61^+$ LPs during pregnancy (Cui et al., 2004; Miyoshi et al., 2001; Vafaizadeh et al., 2010). Even in nulliparous

mice, loss of STAT5 results in impaired differentiation of $CD61^+$ LPs with side-branching defects (Santos et al., 2010; Yamaji et al., 2009), indicating phenocopy between $Id2^{-/-}$ and $Stat5^{-/-}$ mice. Meanwhile, RANKL is a pivotal downstream mediator of progesterone in side branching and luminal differentiation (Beleut et al., 2010; Fernandez-Valdivia et al., 2009; Grimm et al., 2016; Lee et al., 2013; Mukherjee et al., 2010; Obr et al., 2013; Rajaram et al., 2015) and translocates ID2 into the nucleus (Kim et al., 2006, 2011). Obr et al. reported that STAT5 induces the transcription of *Rankl* by cooperating with progesterone (Obr et al., 2013), suggesting that STAT5 induces side branching and luminal lineage differentiation through the RANKL-ID2 pathway. Collectively, ID2 might be a downstream mediator of the progesterone-STAT5 signaling in luminal lineage differentiation and side-branch formation.

In this study, we established a new tissue preparation method that enables the easy observation of ductal trees of mammary glands, and found that most $CD61^+$ LPs reside in budding and side branches but not in TEBs or primary ducts. Based on our results, we suggest that CD61 is a marker of side branches in young virgin mice. Our study provides important insights into the differentiation of progenitors in ductal morphogenesis of mammary glands *in vivo*. Further studies identifying ID2-binding partners and the related molecular mechanisms will help us to understand luminal lineage commitment in developing mammary glands.

MATERIALS AND METHODS
Mice
All animal experiments were conducted using 8-week-old virgin female mice on a FVB/N background, unless otherwise noted (e.g. 12-week-old L1 or 20-week-old mice). '*n*' indicates the number of mice used. The estrus cycle of mice was checked daily at noon, and only mice in diestrus were chosen for experiments. The generation of $Id2^{-/-}$ mice was described previously (Yokota et al., 1999), and mice were a kind gift from Dr Yokota (Department of Molecular Genetics, Graduate School of Medicine, Kyoto University, Japan). *NLS-Id2* Tg mice were generated using a previously characterized method (Kim et al., 2011). Briefly, to construct the vector, HA-tagged murine *NLS-Id2* cDNA was ligated into the *MMTV* long terminal repeat (LTR) plasmid (*pMMTV-NLS-Id2*), which was microinjected into the pronuclei of fertilized one-cell zygotes from FVB/N mice. All mice were maintained at the animal facilities of Seoul National University. All animal experiments were approved by Seoul National University Institutional Animal Care and Use Committee and performed in accordance with the guidelines of the institution.

Vaginal staining
For vaginal staining, PBS-immersed cotton swabs were inserted into the vagina (once a day, at noon). The vaginal secretion was placed on a slide glass, dried, stained with hematoxylin for 30 s, briefly rinsed with 1′ distilled water (DW), and then examined using a fluorescent microscope (Axio Imager A2; Zeiss) equipped with a SPOT Flex camera. All mice were sacrificed at diestrus.

Mammary epithelial cell preparation and single-cell dissociation
Given that large numbers of adipocytes can disrupt the accuracy of experimental results from MECs, we skimmed off the fat from MECs using single-cell dissociation according to the protocol described by STEMCELL Technologies. Briefly, dissected inguinal fat pads were chopped into small pieces and incubated in dissociation medium containing Epicult-B medium (cat. no. 05611 and 05612; STEMCELL Technologies) with 10× collagenase/hyaluronidase (cat. no. 07912; STEMCELL Technologies), 5% fetal bovine serum (FBS; cat. no. SH30070.03; Thermo Fisher Scientific), 10 ng/ml epidermal growth factor (EGF; cat. no. PMG8043; Invitrogen), 10 ng/ml basic fibroblast growth factor (bFGF; cat. no. F0291; Sigma), 10 ng/ml cholera toxin (cat. no. C8052; Sigma) and 0.0004% heparin (cat. no. 07980; STEMCELL Technologies)
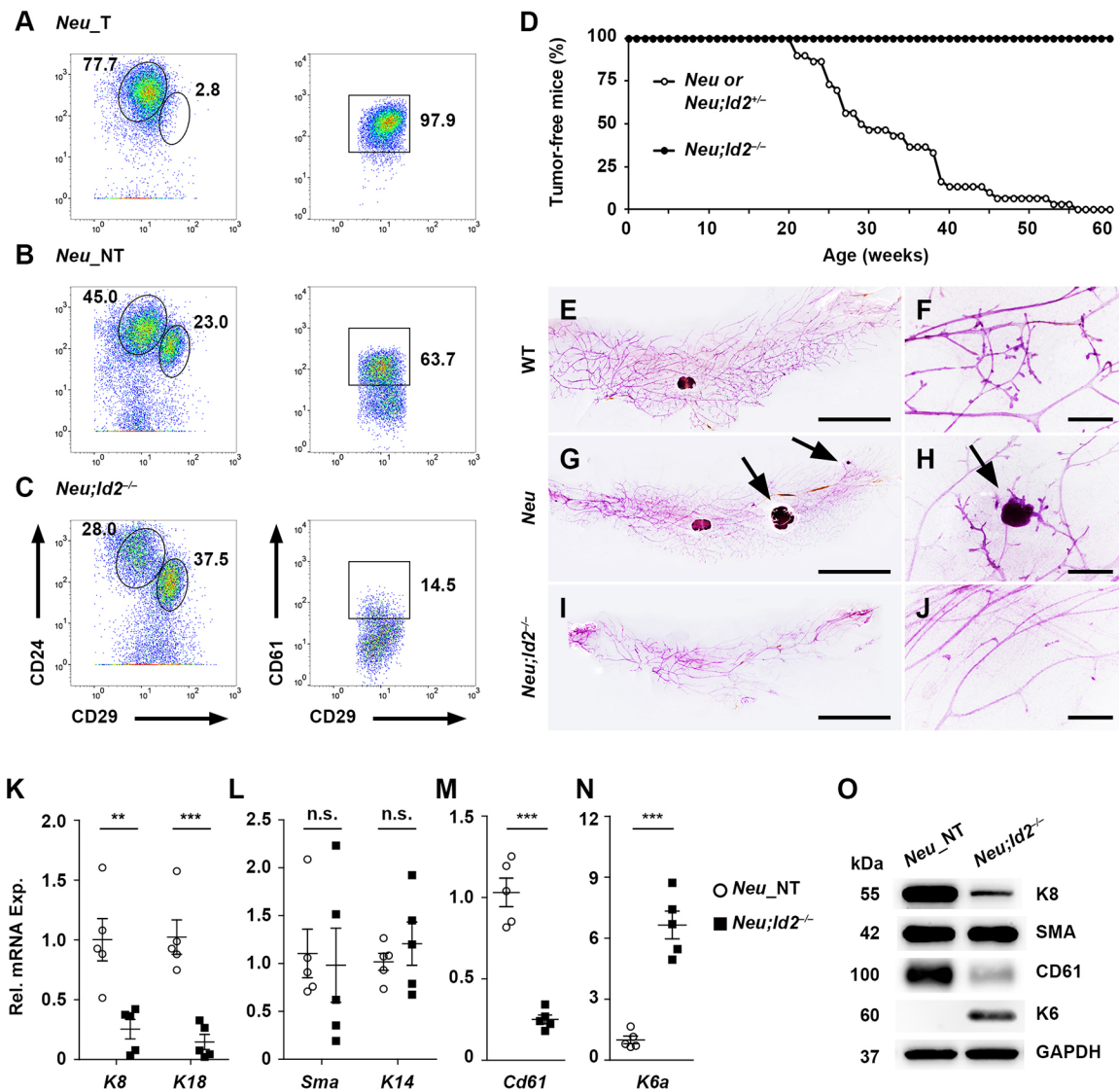
Fig. 7. Lack of CD61⁺ LP-derived tumors in _Id2⁻/⁻_ mice. (A-C) Flow cytometric analysis of T and NT tissues from 28-32-week-old _Neu_ Tg mice and _Neu_ Tg;_Id2⁻/⁻_ mice (_Neu__T and _Neu__NT, respectively). Tumor tissues from _Neu_ Tg mice were derived from CD61⁺ LPs. The slight increases in CD61⁺ LPs in _Neu__NT tissues might result from invisible microadenoma or hyperplastic luminal cells. CD29-CD61 plots were generated from the CD29^midCD24^high luminal population. (D) Percentage of tumor-free mice at the indicated ages. _Neu_ Tg or _Neu_ Tg;_Id2⁺/⁻_ (n=30); _Neu_ Tg;_Id2⁻/⁻_ (n=16). (E-J) C-A-stained inguinal mammary glands from 28-32-week-old wild-type and _Neu_ Tg mice (E-H) and 70-week-old _Neu_ Tg;_Id2⁻/⁻_ mice (I,J). Along with a reduction in side branches, _Neu_ Tg;_Id2⁻/⁻_ mice did not show any sign of tumors. Arrows indicate either tumors or foci. (K-N) qRT-PCR and (O) immunoblotting were used to analyze the expression of mature luminal (K), myoepithelial (L) and progenitor markers (M,N) in _Neu_ Tg MECs isolated from _Neu__NT tissues and _Neu_ Tg;_Id2⁻/⁻_ MECs. The dramatic reduction in luminal lineage markers with the increase in bipotent cell markers in _Neu_ Tg;_Id2⁻/⁻_ MECs indicates that loss of ID2 blocks the differentiation of K6⁺ BPs into luminal lineage cells. n=5, each. Data are means±s.e.m., analyzed by Student's t-test: **P<0.01; ***P<0.001. Scale bars: 1 cm in E,G,I; 1 mm in F,H,J. In A-O, _Neu_ indicates _Neu_ Tg mice. See also Fig. S5.

on a 360° rotator at 37°C for 4 h or 6 h for flow cytometry or RNA/protein extraction, respectively. The suspension was then centrifuged, and the supernatant (mostly adipocytes) was discarded. The pellet was resuspended in red blood cell (RBC) lysis buffer (150 mM NH₄Cl and 10 mM Tris-HCl) and HF solution (Hanks' Balanced Salt Solution plus 2% FBS) at a 4:1 ratio, gently inverted for 5 min at room temperature, and centrifuged at 350×_g_ for 5 min. The supernatant was then discarded. Pellets were resuspended with 0.25% trypsin-ethylenediaminetetraacetic acid (EDTA; cat. no. 15400; Gibco) and mixed well by pipetting for 3 min. Next, pellets were resuspended with a 10:1 ratio of 5 mg/ml dispase (cat. no. 07913; STEMCELL Technologies) and DNase1 (cat. no. 07900; STEMCELL Technologies) for 1 min, followed by HF neutralization. The neutralized solution of MECs was passed through a 40-μm cell strainer (cat. no. 93040; SPL) before centrifugation. Adipocyte-free single MECs were used for subsequent experiments (compared with control groups,

mRNA expression of adipocyte markers was decreased 7.2- to 10.7-fold after dissociation for 6 h; data not shown).

Flow cytometry

After 4 h of incubation and single-cell dissociation, 1×10⁶ MECs were stained for 30 min on ice with the 100 ng of the following primary antibodies: anti-CD24-PE/Cy7 (cat. no. 101821; BioLegend), anti-CD29-APC (cat. no. 102215; BioLegend), anti-CD61-FITC (cat. no. 104305; BioLegend), anti-CD49b-PE (cat. no. 103506; BioLegend), biotinylated anti-CD31 (cat. no. 102404; BioLegend), biotinylated anti-CD45 (cat. no. 103104; BioLegend), biotinylated anti-CD140b (cat. no. 136010; BioLegend) and biotinylated anti-Ter119 (cat. no. 116204; BioLegend). To sort out endothelial cells and leukocytes, MECs were incubated on ice with streptavidin-PerCP (cat. no. 405213; BioLegend) for 15 min. To sort out dead cells, 7-aminoactinomycin D (7-AAD; cat. no. SML1633; Sigma) was
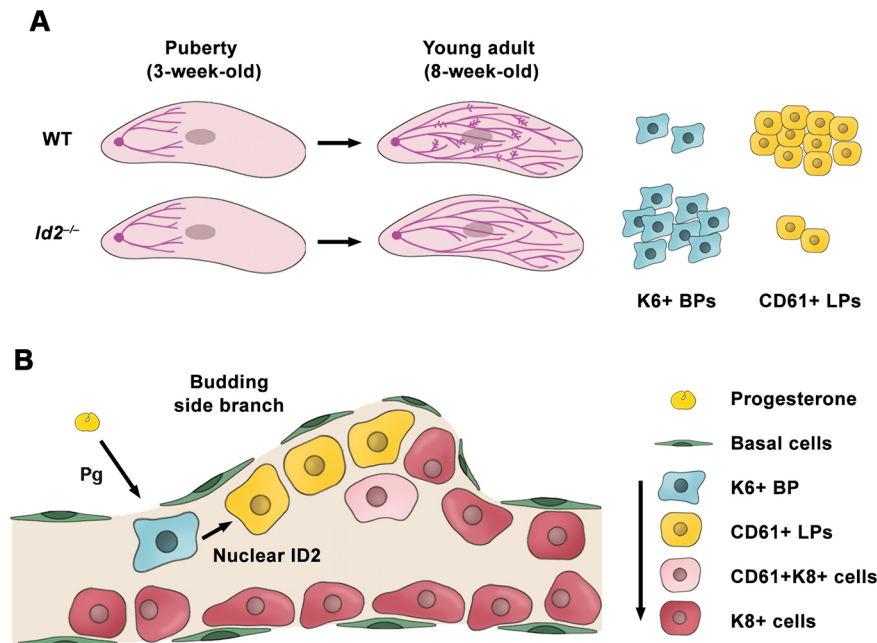
Fig. 8. Schematic view of defects in _Id2^{-/-}_ mice. (A) After puberty, young virgin _Id2^{-/-}_ mice showed severe side-branching defects with increased and decreased numbers of K6^{+} BPs and CD61^{+} LPs, respectively. (B) In putative side-branching points, nuclear ID2 would induce differentiation of K6^{+} BPs into CD61^{+} LPs to form new side branches as a key effector of progesterone.

added (1:1000) to fluorescence-activated cell sorting (FACS) buffer (PBS plus 2% FBS) and incubated for 15 min just before use. Flow cytometry was conducted using FACS Calibur, Canto and Aria3 instruments (BD). We used at least 20,000 cells for CD29-CD24 gating. Data were analyzed by FlowJo software.

RNA extraction, RT-PCR and quantitative PCR
After 6 h of incubation and single-cell dissociation, RNA was extracted from MECs using an RNeasy Mini Kit (cat. no. 74104; Qiagen). Resulting RNAs were reverse transcribed, and qRT-PCR was conducted. qRT-PCR primer sequences were as follows: _Uxt_, 5′-CTGGAACTGACACTGGCTGA-3′ 5′-GATGCAGTCAATGGGGAGAT-3′; β-actin, 5′-TGTTACCAACTGG-GACGACA-3′ 5′-GGGGTGTTGAAGGTCTCAAA-3′; _Gapdh_, 5′-AACT-TTGGCATTGTGGAAGG-3′ 5′-ACACATTGGGGGTAGGAACA-3′; _18 s rRNA_, 5′-CGCGGTTCTATTTTGTTGGT-3′ 5′-AGTCGGCATCGTTTAT-GGTC-3′; _Id2_, 5′-ATCAGCCATTTCACCAGGAG-3′ 5′-TCCCCATGGT-GGGAATAGTA-3′; _K8_, 5′-ATCGAGATCACCACCTACCG-3′ 5′-TGAA-GCCAGGGCTAGTGAGT-3′; _K18_, 5′-AAGGTCTGGAAGCCCAGATT-3′ 5′-CTTGGTGGTGACAACTGTGG-3′; _K19_, 5′-ACCCTCCCGAGATT-ACAACC-3′ 5′-CAAGGCGTGTTCTGTCTCAA-3′; _Sma_, 5′-CTGACAGA-GGCACCACTGAA-3′ 5′-CATCTCCAGAGTCCAGCACA-3′; _K14_, 5′-AG-ATGTGACCTCCACCAACC-3′ 5′-AGGGACAATACAGGGGCTCT-3′; _Cd61_, 5′-GCTCATTGGCCTTGCTACTC-3′ 5′-CCCGGTAGGTGATAT-TGGTG-3′; _K6a_, 5′-ATGAGCAGCTCCCTGTGAGT-3′ 5′-TACGAGG-AAGCCAAGAGCAT-3′; _p15_, 5′-GGCAAGTGGAGACGGTG-3′ 5′-GT-TGGGTTCTGCTCCGTG-3′; _p16_, 5′-CTTCTC- ACCTCGCTTGTCAC-3′ 5′-CGAACTTCACCAAGAAAACC-3′; _p21_, 5′-CTTGCACTCTGGTGT-CTGAG-3′ 5′-GCACTTCAGGGTTTTCTCTTG-3′; _p27_, 5′-AAGGGCC-AACAGAACAGAAG-3′ 5′-GGATGTCCATTCAATGGAGT-3′; β-casein, 5′-AAGCTAAAGCCACCATCCTT-3′ 5′-CAG- CTGGGTCTGAGAAG-AAA-3′; _Wap_, 5′-TGAGGGCACAGAGTGTATCA-3′ 5′-TCGCTGGAG-CATTCTATCTT-3′; α-lactalbumin, 5′-TGAATGGGCCTGTGTTTTAT-3′ 5′-CACGCTATGTCATCATCCAA-3′; _Neu_, 5′-CCCATCAGAGTGATG-TGTGG-3′ 5′-GGGCGACATTCAGAGTCAAT-3′; _Jun_, 5′-TCCCCTAT-CGACATGGAGTC-3′ 5′-TTTTGCGCTTTCAAGGTTTT-3′; _Myc_, 5′-TG-AAGGCTGGATTTCCTTTG-3′ 5′-TTCTCTTCCTCGTCGCAGAT-3′; _Trp53_, 5′-AGAGACCGCCGTACAGAAGA-3′ 5′-CTG- TAGCATGGGC-ATCCTTT-3′; and _Stat3_, 5′-ACCCAACAGCCGCCGT- AG-3′ 5′-CAGAC-TGGTTGTTTCCATTC-3′.

Among the four housekeeping genes (_Uxt_, _Actb_, _Gapdh_ and 18s rRNA) used in this study, _Uxt_ has been reported to be the most stable housekeeping gene for normalizing mRNA levels in bovine mammary tissues (Bionaz and

Loor, 2007). Given that _Uxt_ showed great stability under various conditions, such as age, biological condition (virgin or pregnancy) and experimental condition (short and long dissociation time), we used the _Uxt_ results for normalization of relative mRNA expression as a representative if other housekeeping genes showed similar patterns.

Protein isolation and western blotting
For protein isolation, MECs were dissociated for 6 h and lysed using RIPA buffer (cat. no. 89900; Thermo Fisher Scientific) and a Sonic 130-Watt Ultrasonic Processor (BioExpress). For western blotting, proteins were transferred to polyvinylidene difluoride (PVDF) membranes, and membranes were then blocked with TBS-T (1×TBS plus 0.1% Triton X-100) containing 5% skim milk (cat. no. 232100; BD) at room temperature for 1 h. To detect specific proteins of interest, the following antibodies were used: anti-β-tubulin (cat. no. ab15568; Abcam, 1:2000), anti-β-actin (cat. no. A2066; Sigma, 1:1000), anti-E-cadherin (cat. no. 610182; BD, 1:1000), anti-K8 (cat. no. Troma-1; Developmental Studies Hybridoma Banks, 1:2500), anti-K6 (cat. no. PRB-169P; Covance, 1:1000), anti-SMA (cat. no. ab7817; Abcam, 1:2000) and anti-CD61 (cat. no. 13166; Cell Signaling Technology, Danvers, MA, USA, 1:1000). Horseradish peroxidase (HRP)-conjugated secondary antibodies were then used. Luminescence was detected with a FUSION Solo instrument (Vilber Lourmat).

Carmine-Alum staining
For C-A staining, freshly dissected inguinal fat pads were flattened and stretched on a glass slide as much as possible. To remove lipid but not mammary glands from fat pads, we placed fat pads in Clarke's solution (75% ethanol plus 25% acetic anhydride) for 16-18 h at room temperature. After brief washing with 70% EtOH, fat pads were stained in C-A solution (0.2% carmine, 0.5% aluminium potassium sulfate and 0.02% thymol) for 16-18 h. Destaining was conducted using 2% HCl plus 70% EtOH for 4-6 h. Tissues were then incubated with increasing concentrations of EtOH (70%, 95% and 100%) for dehydration and cleared using xylene. Samples were stored in methyl salicylate. The results were obtained using a Nikon SMZ18 microscope equipped with a Nikon DS-Ri2 camera.

Histological analysis
For histological analysis, inguinal fat pads were fixed with 4% paraformaldehyde overnight at 4°C (for no longer than 24 h) and washed in 1′ DW for 1 day. After EtOH-xylene-paraffin dehydration processing, the tissues were embedded in paraffin and sliced to 5-μm thickness. For immunohistochemistry, rehydrated mammary gland tissues were boiled

at 95°C for 20 min with antigen-retrieval buffer (10 mM Tris plus 1 mM EDTA, pH 9.0) to expose antigenic epitopes. The tissues were incubated with blocking buffer [10% goat serum, 5% bovine serum albumin (BSA) and 0.3% Triton X-100 in PBS] for 2-4 h in a humidified chamber at room temperature and then incubated overnight at 4°C with the following primary antibodies: anti-K8 (cat. no. Troma-1; Developmental Studies Hybridoma Banks, 1:1000), anti-K6 (cat. no. PRB-169P; Covance, 1:1000), anti-SMA (cat. no. ab7817; Abcam, 1:500), anti-CD61 (cat. no. 13166; Cell Signaling Technology, 1:500), anti-p27 (cat. no. sc-1641; Santa Cruz, 1:200), anti-HA (cat. no. sc-7392 and sc-805; Santa Cruz, 1:200 each). Fluorescent probes were affixed using Alexa 488, Alexa 594 and Alexa 647-conjugated antibodies (Invitrogen) targeting the primary antibodies (1:300). Hoechst (cat. no. H3570; Invitrogen, 1:1000) was used to detect nuclei, and slides were mounted with Vectashield (cat. no. H-1000; Vector Laboratories). Immunofluorescence was detected using a confocal laser-scanning microscope (LSM700; Carl Zeiss and TCS SP8; Leica). For H&E staining, the tissues were placed in hematoxylin and eosin for 5 min and 15 s, respectively, with washing using 1′ DW following each step (brief destaining was followed after hematoxylin staining with 1% HCl). After dehydration (increasing concentrations of EtOH, followed by xylene incubation) and mounting (cat. no. 6769007; Thermo Fisher Scientific), tissues were analyzed using a fluorescence microscope (Axio Imager A2; Zeiss) equipped with a SPOT Flex camera.

Flattened tissue preparation
For flattened tissue preparation, freshly dissected inguinal fat pads were washed in PBS briefly and sandwiched between two pieces of 3MM paper (with stretching of the tissues as far as possible). The tissues were stapled firmly to the 3MM paper so that they would not detach from it. The subsequent procedures were the same as described above. Given the horizontal attachment of mammary gland tissues to the 3MM paper, tissues were shrunk only vertically and still had the same horizontal attachment area after undergoing EtOH-xylene-paraffin dehydration. Because not all ducts and side branches elongated in parallel to the cutting plane, it was difficult to find intact branching structures in cross-section with traditional tissue preparation methods. However, this compression enabled detection of more branches per cross-sectional area and yielded a relatively intact side-branch structure.

BrdU incorporation assay
Three hours before sacrifice, mice were intraperitoneally injected with BrdU (50 µg/g body weight; cat. no. B5002; Sigma). For immunofluorescence, we used anti-BrdU (cat. no. ab92837; Abcam) as a primary antibody. Secondary antibodies were the same as described in the Histological analysis section.

Whole-tissue clearing and 3D imaging
For 3D imaging, we performed the CUBIC method as previously reported (Lloyd-Lewis et al., 2016; Susaki et al., 2014) with minor modifications. Briefly, mammary fat pads were fixed with 4% paraformaldehyde overnight at 4°C and 1 h at room temperature, and washed with PBS (1 h×2 times). The tissues were incubated in Reagent 1 [25% (w/w) urea, 25% (w/w) N,N,N',N'-tetrakis(2-hydroxypropyl)ethylenediamine, 15% (w/w) triton x-100 in distilled water] for 3 days at 37°C, and washed with PBS (1 h) and with 0.1% Triton X-100 in PBS (PBST) (1 h×2 times) at room temperature. The tissues were incubated with blocking buffer (10% goat serum in 0.5% PBST) overnight at 4°C, and then incubated for 4 days at 4°C with gentle rocking and the following primary antibodies: anti-K8 (cat. no. Troma-1; Developmental Studies Hybridoma Banks, 1:1000) and anti-CD61 (cat. no. 13166; Cell Signaling Technology, 1:500). Fluorescent probes were affixed using Alexa 488 and Alexa 594-conjugated antibodies (Invitrogen) targeting the primary antibodies (1:300) for 2 days at 4°C with gentle rocking, and Hoechst (cat. no. H3570; Invitrogen, 1:1000) was used to detect nuclei. A PBST (0.3%) wash followed each antibody and Hoechst incubation (1 h×3 times). The tissues were incubated in Reagent 2 [44% (w/w) sucrose, 22% (w/w) urea, 9% (w/w) 2,2′,2″-nitrilotriethanol, 0.1% (w/w) triton x-100 in distilled water] for tissue clearing at least 4 days at 37°C with gentle rocking. K8 was detected easily after 1-2 days of clearing, but CD61

begin to be detected after 4 days clearing. Immunofluorescence was detected using a confocal laser-scanning microscope (TCS SP8; Leica). Movies 1 and 2 comprise 1000 frames (60 frames per second).

Cell lines and immunocytochemistry
For ICC, we used the HC11 cell line that we purchased from ATCC. After clearance for *Mycoplasma* contamination, HC11 cells were incubated with RPMI 1640 medium (cat. no. SH30027.01; Hyclone) containing 10% FBS, 10 ng/ml EGF, 100× GlutaMAX (cat. no. 35050; Gibco), 5 µg/ml insulin (cat. no. 91077C-100MG; Sigma) and 100× Antibiotic-Antimycotic (cat. no. 15240; Gibco) at 37°C in an incubator containing 5% CO$_2$. For vector transfection, we used *pcDNA-HA-Id2*, and *NLS-Id2* vectors. We mixed vectors (2 µg each) and 8 µg polyethylenimine (PEI; cat. no. 23966-2; Polyscience) with 200 µl prewarmed Opti-MEM (cat. no. 11058021; Gibco) and incubated the resulting solution for 10 min at room temperature. For transfection with Metafectene reagent (cat. no. T020-1.0; Biontex), we mixed vectors (3 µg, each) and 9 µg Metafectene with 100 µl prewarmed Opti-MEM and incubated the resulting solution for 10 min at room temperature. This mixture was then added to HC11 cells in 6-well plates with non-RPMI 1640 medium and incubated for 4-6 h at 37°C in an incubator containing 5% CO$_2$. The medium was then replaced with complete RPMI 1640 medium, and the cells were incubated for an additional 2 days. For CD61$^-$CD49b$^-$ single-cell sorting, mammary epithelial cells in inguinal fat pads were dissociated and stained with antibodies, as described in the flow cytometry section above. Flow cytometry was conducted using FACS AriaIII instruments (BD), and sorted single cells were spun down on glass slides using Cytospin4 (Thermo Fisher Scientific). For ICC, cells were fixed for 30 min on ice with 4% PFA and permeabilized for 30 min at room temperature with 0.2% PBST. After brief washing with 0.1% PBST, the cells were incubated with blocking buffer (2% BSA in 0.1% PBST) for 30 min and then incubated overnight at 4°C with the following primary antibodies: anti-CD61 (cat. no. sc-365679; Santa Cruz, 1:500), anti-K6 (cat. no. PRB-169P; Covance, 1:1000) and anti-HA (cat. no. sc-7392 and sc-805; Santa Cruz, 1:200 each). Fluorescent probes were affixed using Alexa 488-conjugated and Alexa 594-conjugated antibodies (Invitrogen) against primary antibodies (1:300). Hoechst (1:1000) was used to detect nuclei, and slides were mounted with Vectashield (cat. no. H-1000; Vector Laboratories). Immunofluorescence was detected using a confocal laser-scanning microscope (TCS SP8; Leica).

Transplantation
Inguinal fat pads from 8-week-old wild-type and *Id2*$^{-/-}$ mice were dissected and minced in chopping buffer (dissociation medium without collagenase/hyaluronidase and cholera toxin). Approximately 1 mm^3 of the minced inguinal fat pads from wild-type and *Id2*$^{-/-}$ mice was transplanted into the left and right cleared fat pads of 3-week-old virgin wild-type mice, respectively (Grimm et al., 2006; Naylor and Ormandy, 2002; Welm et al., 2008). To show ductal elongation, we implanted MECs at the edge of each of the cleared fat pads of the recipient mice. After 8-10 weeks, ductal outgrowth was compared between pads in each recipient mouse by C-A staining.

Ovariectomy and hormone administration
For observation of outgrowth of side branches, 5-week-old mice were anesthetized by intraperitoneal injection of 250 µg/g 2,2,2-tribromoethanol (Avertin; cat. no. T48402-25G; Sigma) and ovariectomized. Given that side branches were evident in 6-week-old wild-type virgin mice, we used 5-week-old mice to avoid confusing newly formed side branches induced by ID2 from natural side branching induced by endogenous hormones. After a 3-week recovery period (Ingberg et al., 2012), a 2-cm silastic tube (cat. no. 508-009; Dow Corning) with 17β-estradiol (cat. no. E8875-1G; Sigma) and progesterone (cat. no. P0130-25G; Sigma), with both ends blocked using 3-mm wooden caps, was implanted in each mouse; 17β-estradiol and progesterone were dissolved in corn oil (cat. no. C8267-500ML; Sigma) at concentrations of 30 µg/ml and 1 mg/ml, respectively, based on references (Aupperlee et al., 2013; Joshi et al., 2010; Strom et al., 2012). After an additional 1 week of hormone administration, inguinal mammary glands were used for quantification of the number of branches

with C-A staining. For flow cytometry and analysis of luminal lineage differentiation, 3-week-old mice were ovariectomized to minimize the effects of endogenous ovarian hormones on luminal lineage differentiation. After a 3-week recovery period, silastic tubes with 17b-estradiol and/or progesterone were implanted. After 3 weeks of hormone administration, mammary glands were used for flow cytometry to examine luminal lineage differentiation.

Statistical analysis

All statistical analyses were performed using GraphPad Prism 5 (GraghPadSoftware) and Excel 2016 (Microsoft). All error bars represent the standard error of the mean (s.e.m.). Data were analyzed using a two-way ANOVA analysis and a two-sample t-test (for a difference in means). A two-way ANOVA analysis was performed for the data presented in Fig. 6E and Fig. S5C. A two-sample t-test was performed for the data presented in Figs 1I,P; 2B,C,M,P,Q; 4L,N,P,Q; 5C,H,K; 6G and 7K-N, and Figs S1J,K; S2B-D; S3I; S4G,H and S5B-E,G. A P-value <0.05 was considered statistically significant at the 95% confidence level. The number of biological (nontechnical) replicates for each experiment is indicated in the figure legends. All representative images shown are from experiments that have been performed in triplicate at least.

References

Asselin-Labat, M.-L., Sutherland, K. D., Barker, H., Thomas, R., Shackleton, M., Forrest, N. C., Hartley, L., Robb, L., Grosveld, F. G., van der Wees, J. et al. (2007). Gata-3 is an essential regulator of mammary-gland morphogenesis and luminal-cell differentiation. *Nat. Cell Biol.* **9**, 201-209.

Atwood, C. S., Hovey, R. C., Glover, J. P., Chepko, G., Ginsburg, E., Robison, W. G. and Vonderhaar, B. K. (2000). Progesterone induces side-branching of the ductal epithelium in the mammary glands of peripubertal mice. *J. Endocrinol.* **167**, 39-52.

Aupperlee, M. D., Leipprandt, J. R., Bennett, J. M., Schwartz, R. C. and Haslam, S. Z. (2013). Amphiregulin mediates progesterone-induced mammary ductal development during puberty. *Breast Cancer Res.* **15**, R44.

Beleut, M., Rajaram, R. D., Caikovski, M., Ayyanan, A., Germano, D., Choi, Y., Schneider, P. and Brisken, C. (2010). Two distinct mechanisms underlie progesterone-induced proliferation in the mammary gland. *Proc. Natl. Acad. Sci. USA* **107**, 2989-2994.

Best, S. A., Hutt, K. J., Fu, N. Y., Vaillant, F., Liew, S. H., Hartley, L., Scott, C. L., Lindeman, G. J. and Visvader, J. E. (2014). Dual roles for Id4 in the regulation of estrogen signaling in the mammary gland and ovary. *Development* **141**, 3159-3164.

Bionaz, M. and Loor, J. J. (2007). Identification of reference genes for quantitative real-time PCR in the bovine mammary gland during the lactation cycle. *Physiol. Genomics* **29**, 312-319.

Brisken, C. (2013). Progesterone signalling in breast cancer: a neglected hormone coming into the limelight. *Nat. Rev. Cancer* **13**, 385-396.

Brisken, C. and Duss, S. (2007). Stem cells and the stem cell niche in the breast: an integrated hormonal and developmental perspective. *Stem Cell Rev.* **3**, 147-156.

Brisken, C., Heineman, A., Chavarria, T., Elenbaas, B., Tan, J., Dey, S. K., McMahon, J. A., McMahon, A. P. and Weinberg, R. A. (2000). Essential function of Wnt-4 in mammary gland development downstream of progesterone signaling. *Genes Dev.* **14**, 650-654.

Bu, W., Chen, J., Morrison, G. D., Huang, S., Creighton, C. J., Huang, J., Chamness, G. C., Hilsenbeck, S. G., Roop, D. R., Leavitt, A. D. et al. (2011). Keratin 6a marks mammary bipotential progenitor cells that can give rise to a unique tumor model resembling human normal-like breast cancer. *Oncogene* **30**, 4399-4409.

Chakrabarti, R., Wei, Y., Romano, R.-A., DeCoste, C., Kang, Y. and Sinha, S. (2012). Elf5 regulates mammary gland stem/progenitor cell fate by influencing notch signaling. *Stem Cells* **30**, 1496-1508.

Choi, Y. S., Chakrabarti, R., Escamilla-Hernandez, R. and Sinha, S. (2009). Elf5 conditional knockout mice reveal its role as a master regulator in mammary alveolar development: failure of Stat5 activation and functional differentiation in the absence of Elf5. *Dev. Biol.* **329**, 227-241.

Cui, Y., Riedlinger, G., Miyoshi, K., Tang, W., Li, C., Deng, C.-X., Robinson, G. W. and Hennighausen, L. (2004). Inactivation of Stat5 in mouse mammary epithelium during pregnancy reveals distinct functions in cell proliferation, survival, and differentiation. *Mol. Cell. Biol.* **24**, 8037-8047.

Davis, F. M., Lloyd-Lewis, B., Harris, O. B., Kozar, S., Winton, D. J., Muresan, L. and Watson, C. J. (2016). Single-cell lineage tracing in the mammary gland reveals stochastic clonal dispersion of stem/progenitor cell progeny. *Nat. Commun.* **7**, 13053.

de Candia, P., Benera, R. and Solit, D. B. (2004). A role for Id proteins in mammary gland physiology and tumorigenesis. *Adv. Cancer Res.* **92**, 81-94.

Desgrosellier, J. S., Lesperance, J., Seguin, L., Gozo, M., Kato, S., Franovic, A., Yebra, M., Shattil, S. J. and Cheresh, D. A. (2014). Integrin alphavbeta3 drives slug activation and stemness in the pregnant and neoplastic mammary gland. *Dev. Cell* **30**, 295-308.

Dong, J., Huang, S., Caikovski, M., Ji, S., McGrath, A., Custorio, M. G., Creighton, C. J., Maliakkal, P., Bogoslovskaia, E., Du, Z. et al. (2011). ID4 regulates mammary gland development by suppressing p38MAPK activity. *Development* **138**, 5247-5256.

Fata, J. E., Kong, Y.-Y., Li, J., Sasaki, T., Irie-Sasaki, J., Moorehead, R. A., Elliott, R., Scully, S., Voura, E. B., Lacey, D. L. et al. (2000). The osteoclast differentiation factor osteoprotegerin-ligand is essential for mammary gland development. *Cell* **103**, 41-50.

Fernandez-Valdivia, R., Mukherjee, A., Ying, Y., Li, J., Paquet, M., DeMayo, F. J. and Lydon, J. P. (2009). The RANKL signaling axis is sufficient to elicit ductal side-branching and alveologenesis in the mammary gland of the virgin mouse. *Dev. Biol.* **328**, 127-139.

Fu, N. Y., Rios, A. C., Pal, B., Law, C. W., Jamieson, P., Liu, R., Vaillant, F., Jackling, F., Liu, K. H., Smyth, G. K. et al. (2017). Identification of quiescent and spatially restricted mammary stem cells that are hormone responsive. *Nat. Cell Biol.* **19**, 164-176.

Gajewska, M., Zielniok, K. and Motyl, T. (2013). Autophagy in development and remodelling of mammary gland. In Autophagy – A Double-Edged Sword (ed. Y. Bailly), pp. 443-464. London: IntechOpen.

Grimm, S. L., Bu, W., Longley, M. A., Roop, D. R., Li, Y. and Rosen, J. M. (2006). Keratin 6 is not essential for mammary gland development. *Breast Cancer Res.* **8**, R29.

Grimm, S. L., Hartig, S. M. and Edwards, D. P. (2016). Progesterone receptor signaling mechanisms. *J. Mol. Biol* **428**, 3831-3849.

Hannezo, E., Scheele, C., Moad, M., Drogo, N., Heer, R., Sampogna, R. V., van Rheenen, J. and Simons, B. D. (2017). A unifying theory of branching morphogenesis. *Cell* **171**, 242-255.e227.

Hennighausen, L. and Robinson, G. W. (2005). Information networks in the mammary gland. *Nat. Rev. Mol. Cell Biol.* **6**, 715-725.

Howlin, J., McBryan, J. and Martin, F. (2006). Pubertal mammary gland development: insights from mouse models. *J. Mammary Gland Biol. Neoplasia* **11**, 283-297.

Ingberg, E., Theodorsson, A., Theodorsson, E. and Strom, J. O. (2012). Methods for long-term 17beta-estradiol administration to mice. *Gen. Comp. Endocrinol.* **175**, 188-193.

Joshi, P. A., Jackson, H. W., Beristain, A. G., Di Grappa, M. A., Mote, P. A., Clarke, C. L., Stingl, J., Waterhouse, P. D. and Khokha, R. (2010). Progesterone induces adult mammary stem cell expansion. *Nature* **465**, 803-807.

Junankar, S., Baker, L. A., Roden, D. L., Nair, R., Elsworth, B., Gallego-Ortega, D., Lacaze, P., Cazet, A., Nikolic, I., Teo, W. S. et al. (2015). ID4 controls mammary stem cells and marks breast cancers with a stem cell-like phenotype. *Nat. Commun.* **6**, 6548.

Kim, N.-S., Kim, H.-J., Koo, B.-K., Kwon, M.-C., Kim, Y.-W., Cho, Y., Yokota, Y., Penninger, J. M. and Kong, Y.-Y. (2006). Receptor activator of NF-kappaB ligand regulates the proliferation of mammary epithelial cells via Id2. *Mol. Cell. Biol.* **26**, 1002-1013.

Kim, N.-S., Kim, H.-T., Kwon, M.-C., Choi, S.-W., Kim, Y.-Y., Yoon, K.-J., Koo, B.-K., Kong, M.-P., Shin, J., Cho, Y. et al. (2011). Survival and differentiation of mammary epithelial cells in mammary gland development require nuclear retention of Id2 due to RANK signaling. Mol. Cell. Biol. 31, 4775-4788.

Kouros-Mehr, H., Slorach, E. M., Sternlicht, M. D. and Werb, Z. (2006). GATA-3 maintains the differentiation of the luminal cell fate in the mammary gland. Cell 127, 1041-1055.

Lee, H. J., Gallego-Ortega, D., Ledger, A., Schramek, D., Joshi, P., Szwarc, M. M., Cho, C., Lydon, J. P., Khokha, R., Penninger, J. M. et al. (2013). Progesterone drives mammary secretory differentiation via RankL-mediated induction of Elf5 in luminal progenitor cells. Development 140, 1397-1401.

Lloyd-Lewis, B., Davis, F. M., Harris, O. B., Hitchcock, J. R., Lourenco, F. C., Pasche, M. and Watson, C. J. (2016). Imaging the mammary gland and mammary tumours in 3D: optical tissue clearing and immunofluorescence methods. Breast Cancer Res. 18, 127.

Lo, P.-K., Kanojia, D., Liu, X., Singh, U. P., Berger, F. G., Wang, Q. and Chen, H. (2012). CD49f and CD61 identify Her2/neu-induced mammary tumor-initiating cells that are potentially derived from luminal progenitors and maintained by the integrin-TGFbeta signaling. Oncogene 31, 2614-2626.

Lyden, D., Young, A. Z., Zagzag, D., Yan, W., Gerald, W., O'Reilly, R., Bader, B. L., Hynes, R. O., Zhuang, Y., Manova, K. et al. (1999). Id1 and Id3 are required for neurogenesis, angiogenesis and vascularization of tumour xenografts. Nature 401, 670-677.

Lydon, J. P., DeMayo, F. J., Funk, C. R., Mani, S. K., Hughes, A. R., Montgomery, C. A., Jr, Shyamala, G., Conneely, O. M. and O'Malley, B. W. (1995). Mice lacking progesterone receptor exhibit pleiotropic reproductive abnormalities. Genes Dev. 9, 2266-2278.

Miyoshi, K., Shillingford, J. M., Smith, G. H., Grimm, S. L., Wagner, K.-U., Oka, T., Rosen, J. M., Robinson, G. W. and Hennighausen, L. (2001). Signal transducer and activator of transcription (Stat) 5 controls the proliferation and differentiation of mammary alveolar epithelium. J. Cell Biol. 155, 531-542.

Miyoshi, K., Meyer, B., Gruss, P., Cui, Y., Renou, J.-P., Morgan, F. V., Smith, G. H., Reichenstein, M., Shani, M., Hennighausen, L. et al. (2002). Mammary epithelial cells are not able to undergo pregnancy-dependent differentiation in the absence of the helix-loop-helix inhibitor Id2. Mol. Endocrinol. 16, 2892-2901.

Mori, S., Nishikawa, S. I. and Yokota, Y. (2000). Lactation defect in mice lacking the helix-loop-helix inhibitor Id2. EMBO J. 19, 5772-5781.

Mori, S., Inoshima, K., Shima, Y., Schmidt, E. V. and Yokota, Y. (2003). Forced expression of cyclin D1 does not compensate for Id2 deficiency in the mammary gland. FEBS Lett. 551, 123-127.

Mukherjee, A., Soyal, S. M., Li, J., Ying, Y., He, B., DeMayo, F. J. and Lydon, J. P. (2010). Targeting RANKL to a specific subset of murine mammary epithelial cells induces ordered branching morphogenesis and alveologenesis in the absence of progesterone receptor expression. FASEB J. 24, 4408-4419.

Naylor, M. J. and Ormandy, C. J. (2002). Mouse strain-specific patterns of mammary epithelial ductal side branching are elicited by stromal factors. Dev. Dyn. 225, 100-105.

Norton, J. D., Deed, R. W., Craggs, G. and Sablitzky, F. (1998). Id helix-loop-helix proteins in cell growth and differentiation. Trends Cell Biol. 8, 58-65.

Oakes, S. R., Naylor, M. J., Asselin-Labat, M.-L., Blazek, K. D., Gardiner-Garden, M., Hilton, H. N., Kazlauskas, M., Pritchard, M. A., Chodosh, L. A., Pfeffer, P. L. et al. (2008). The Ets transcription factor Elf5 specifies mammary alveolar cell fate. Genes Dev. 22, 581-586.

Obr, A. E., Grimm, S. L., Bishop, K. A., Pike, J. W., Lydon, J. P. and Edwards, D. P. (2013). Progesterone receptor and Stat5 signaling cross talk through RANKL in mammary epithelial cells. Mol. Endocrinol. 27, 1808-1824.

Parrinello, S., Lin, C. Q., Murata, K., Itahana, Y., Singh, J., Krtolica, A., Campisi, J. and Desprez, P. Y. (2001). Id-1, ITF-2, and Id-2 comprise a network of helix-loop-helix proteins that regulate mammary epithelial cell proliferation, differentiation, and apoptosis. J. Biol. Chem. 276, 39213-39219.

Prat, A. and Perou, C. M. (2009). Mammary development meets cancer genomics. Nat. Med. 15, 842-844.

Rajaram, R. D., Buric, D., Caikovski, M., Ayyanan, A., Rougemont, J., Shan, J., Vainio, S. J., Yalcin-Ozuysal, O. and Brisken, C. (2015). Progesterone and Wnt4 control mammary stem cells via myoepithelial crosstalk. EMBO J. 34, 641-652.

Robinson, G. W. (2007). Cooperation of signalling pathways in embryonic mammary gland development. Nat. Rev. Genet. 8, 963-972.

Šale, S., Lafkas, D. and Artavanis-Tsakonas, S. (2013). Notch2 genetic fate mapping reveals two previously unrecognized mammary epithelial lineages. Nat. Cell Biol. 15, 451-460.

Santos, S. J., Haslam, S. Z. and Conrad, S. E. (2010). Signal transducer and activator of transcription 5a mediates mammary ductal branching and proliferation in the nulliparous mouse. Endocrinology 151, 2876-2885.

Scheele, C. L., Hannezo, E., Muraro, M. J., Zomer, A., Langedijk, N. S., van Oudenaarden, A., Simons, B. D. and van Rheenen, J. (2017). Identity and dynamics of mammary stem cells during branching morphogenesis. Nature 542, 313-317.

Shackleton, M., Vaillant, F., Simpson, K. J., Stingl, J., Smyth, G. K., Asselin-Labat, M. L., Wu, L., Lindeman, G. J. and Visvader, J. E. (2006). Generation of a functional mammary gland from a single stem cell. Nature 439, 84-88.

Shehata, M., Teschendorff, A., Sharp, G., Novcic, N., Russell, I. A., Avril, S., Prater, M., Eirew, P., Caldas, C., Watson, C. J. et al. (2012). Phenotypic and functional characterisation of the luminal cell hierarchy of the mammary gland. Breast Cancer Res. 14, R134.

Smith, G. H., Mehrel, T. and Roop, D. R. (1990). Differential keratin gene expression in developing, differentiating, preneoplastic, and neoplastic mouse mammary epithelium. Cell Growth Differ. 1, 161-170.

Soyal, S., Ismail, P. M., Li, J., Mulac-Jericevic, B., Conneely, O. M. and Lydon, J. P. (2002). Progesterone's role in mammary gland development and tumorigenesis as disclosed by experimental mouse genetics. Breast Cancer Res. 4, 191-196.

Sternlicht, M. D., Kouros-Mehr, H., Lu, P. and Werb, Z. (2006). Hormonal and local control of mammary branching morphogenesis. Differentiation 74, 365-381.

Strom, J. O., Theodorsson, A., Ingberg, E., Isaksson, I. M. and Theodorsson, E. (2012). Ovariectomy and 17beta-estradiol replacement in rats and mice: a visual demonstration. J. Vis. Exp. 64, e4013.

Sun, P., Yuan, Y., Li, A., Li, B. and Dai, X. (2010). Cytokeratin expression during mouse embryonic and early postnatal mammary gland development. Histochem. Cell Biol. 133, 213-221.

Susaki, E. A., Tainaka, K., Perrin, D., Kishino, F., Tawara, T., Watanabe, T. M., Yokoyama, C., Onoe, H., Eguchi, M., Yamaguchi, S. et al. (2014). Whole-brain imaging with single-cell resolution using chemical cocktails and computational analysis. Cell 157, 726-739.

Vafaizadeh, V., Klemmt, P., Brendel, C., Weber, K., Doebele, C., Britt, K., Grez, M., Fehse, B., Desrivieres, S. and Groner, B. (2010). Mammary epithelial reconstitution with gene-modified stem cells assigns roles to Stat5 in luminal alveolar cell fate decisions, differentiation, involution, and mammary tumor formation. Stem Cells 28, 928-938.

Vaillant, F., Asselin-Labat, M.-L., Shackleton, M., Forrest, N. C., Lindeman, G. J. and Visvader, J. E. (2008). The mammary progenitor marker CD61/beta3 integrin identifies cancer stem cells in mouse models of mammary tumorigenesis. Cancer Res. 68, 7711-7717.

Visvader, J. E. and Stingl, J. (2014). Mammary stem cells and the differentiation hierarchy: current status and perspectives. Genes Dev. 28, 1143-1158.

Welm, B. E., Dijkgraaf, G. J. P., Bledau, A. S., Welm, A. L. and Werb, Z. (2008). Lentiviral transduction of mammary stem cells for analysis of gene function during development and cancer. Cell Stem Cell 2, 90-102.

Woodward, W. A., Chen, M. S., Behbod, F. and Rosen, J. M. (2005). On mammary stem cells. J. Cell Sci. 118, 3585-3594.

Yamaji, D., Na, R., Feuermann, Y., Pechhold, S., Chen, W., Robinson, G. W. and Hennighausen, L. (2009). Development of mammary luminal progenitor cells is controlled by the transcription factor STAT5A. Genes Dev. 23, 2382-2387.

Yokota, Y., Mansouri, A., Mori, S., Sugawara, S., Adachi, S., Nishikawa, S.-I. and Gruss, P. (1999). Development of peripheral lymphoid organs and natural killer cells depends on the helix-loop-helix inhibitor Id2. Nature 397, 702-706.

Yokota, Y., Mori, S., Narumi, O. and Kitajima, K. (2001). In vivo function of a differentiation inhibitor, Id2. IUBMB Life 51, 207-214.